A dual DNA/RNA-binding factor regulates co-transcriptional splicing through target RNA interaction and modulates splicing factor dynamics

Mukulika Ray*, Julia Zaborowsky*, Pranav Mahableshwarkar, Smriti Vaidyanathan, Jasmine Shum, Annie Huang, Renjith Viswanathan, Isabelle Pilo, Victoria Chen, Kaitlyn Cortez, Ashley M. Conard, Szu-Huan Wang, Victoria Johnson, Noah Wake, Alexander E. Conicella, Ryan Puterbaugh, Nicolas L. Fawzi†, and Erica Larschan†

* Co-first Authors

†Co-Corresponding authors

Summary

How RNA splicing events are targeted to the correct genomic locations in specific cellular contexts to generate context-specific transcript diversity and prevent deleterious cryptic splicing remains very poorly understood. We show that a functionally conserved GA-rich DNA-binding transcription factor (TF), CLAMP, targets distinct RNA molecules in male and female cells to precisely regulate sex-specific splicing events through physical and functional interactions with RNA and RNA-binding proteins (RBPs). The prion-like domain of CLAMP (PrLD) and a stem-loop region in the target RNA are important for CLAMP-RNA interaction. Moreover, the CLAMP PrLD domain regulates sex-specific splicing by modulating the dynamics of an hnRNPA2/B1 family protein that regulates alternative splicing. Thus, we demonstrate that a TF targets co-transcriptional splicing to the correct genomic locations by directly linking DNA binding sites to RNA targets and modulating the dynamics of RBP partners that drive alternative splicing.

Introduction

Mechanisms that drive precise co-transcriptional alternative splicing at thousands of genomic loci are critical for establishing sex- and cell-type-specific transcriptome diversity and preventing deleterious cryptic splicing events that often occur in disease contexts[1]. Chromatin-bound transcription factors (TFs) and RNA-binding proteins (RBPs) co-transcriptionally regulate alternative splicing[2–5]. Most TFs bind DNA and RNA[6–8] and interact with diverse RBPs[9,10]. However, the mechanisms by which TFs and RBPs coordinate transcription and alternative splicing at specific genomic locations in a particular cell type to drive specific alternative splicing events and prevent deleterious cryptic splicing remain poorly understood. Also, how interactions between TFs, RNA, and RBPs generate the specific alternatively spliced transcripts essential for making developmental decisions remains unknown. We hypothesized that a subset of TFs are critical for targeting the correct co-transcriptional splicing events to specific genomic locations due to their unique ability to bind chromatin, RNA, and spliceosomal RBPs at intron-exon boundaries.

We test this hypothesis by defining the role of the GA-binding TF CLAMP (chromatin-linked adapter for MSL Proteins) in targeting sex-specific splicing to the correct genomic locations on chromatin in *Drosophila* because we can simultaneously genetically manipulate the system, conduct high-throughput genomic experiments *in vivo,* and performing live imaging experiments in living tissue. CLAMP has several properties that suggest that it could target sex-specific alternative splicing events to chromatin: 1) CLAMP binds to specific GA-enriched DNA motifs via its mapped DNA binding domain, and its binding sites differ between males and females[11–14]; 2) CLAMP is a pioneer TF that regulates sex-specific splicing in embryos at genes where it does not regulate transcription[15]; 3) CLAMP is enriched at the intronic regions of CLAMP-dependent sex-specifically spliced genes[12,15]; 4) CLAMP is associated with RBPs that are spliceosome components[10].

Here, we combine diverse *in vivo* and *in vitro* approaches to define a new mechanism by which a TF can regulate co-transcriptional splicing. We define direct CLAMP-RNA interactions and

63 compare them with CLAMP-DNA interactions to identify associations between TF-DNA and TF-
64 RNA binding at genes regulated by CLAMP in sex-specific alternative splicing. We have
65 identified essential protein and RNA domains that promote direct CLAMP-RNA interactions using
66 NMR (Nuclear Magnetic Resonance) spectroscopy and RNA-protein EMSAs (Electrophoretic
67 Mobility Shift Assays). Furthermore, we determined that CLAMP directly regulates the
68 biophysical properties of Hrp38, its RBP interaction partner, which is an hnRNPA2/B1 homolog
69 known to regulate alternative splicing as part of nuclear splicing condensates. Thus, overall, our
70 data support a model in which transcription factors with both DNA and RNA binding capacity can
71 target unique RNA molecules to specific genomic locations and alter the biophysical properties of
72 RBP partner proteins to regulate context-specific alternative splicing.
73
74
75 **Results**
76
77 **CLAMP binds RNA on chromatin**
78
79 Because CLAMP is a DNA-binding protein enriched at the intronic regions of CLAMP-dependent
80 sex-specifically spliced genes, which interacts with multiple splicing factors[12,15], we hypothesized
81 that CLAMP functions as a regulator of co-transcriptional splicing. To test this hypothesis, we first
82 investigated whether CLAMP regulates sex-specific splicing by directly interacting with target
83 RNAs. Therefore, we defined RNA species interacting with CLAMP at high resolution across
84 different cellular compartments: the nucleoplasm vs. chromatin. If we identified CLAMP-RNA
85 interactions in the chromatin fraction involving RNAs that require CLAMP for their alternative
86 splicing, this would support a model in which CLAMP targets co-transcriptional splicing to
87 specific genomic loci. To further define a potential co-transcriptional function for CLAMP, we
88 wanted to identify the spatial distribution of CLAMP RNA binding with respect to its DNA
89 binding across the genome by comparing CLAMP-RNA binding sites with CLAMP DNA binding
90 sites.
91
92 To achieve these objectives, we performed fractionation iCLIP (**i**ndividual-nucleotide resolution
93 **C**ross**L**inking and **I**mmuno**P**recipitation) to identify CLAMP RNA targets using anti-CLAMP

94 antibody in chromatin fractions (ChF) and nucleoplasmic fractions (NF) of male (S2) and female
95 (Kc) *Drosophila* cell lines (Fig 1A). Kc and S2 cells are well-established cell lines for studying
96 sex-specific processes such as dosage compensation[16,17].
97
98 We found that most CLAMP interactions with RNA occur on chromatin (91.9% in males and
99 58.4% in females), with unique sex-specific targets, and that more RNA transcripts bind to
100 CLAMP in males (N=654) than in females (N=286) (Fig 1B, Table 1a). Interestingly, CLAMP
101 also directly interacts with spliceosomal RNAs sex-specifically (Table 1a). In the male chromatin
102 fraction, CLAMP interacts with the catalytic step 2 spliceosome consisting of U2, U5, and U6
103 snRNAs (FDR:1.7E-3). In contrast, the female chromatin fraction is enriched for transcripts that
104 encode proteins that bind to the U1-U2 snRNAs (FDR:1.1E-2), suggesting that CLAMP may
105 regulate splicing differently in males and females by interacting with different spliceosomal
106 RNAs.
107
108 Next, we asked how the CLAMP interaction with DNA correlates with its interaction with RNA
109 on chromatin. Therefore, we used Bindcompare, a tool we developed for comparing protein
110 binding to nucleic acids18, to plot the frequency of CLAMP RNA binding peaks on chromatin
111 within a region ±1 kb of the closest CLAMP DNA binding peak. Using Bindcompare, we defined
112 the following categories of binding sites: a) complete overlap (CRO) of RNA peaks with DNA
113 peaks; b) partial overlap of RNA peak with the ends of a DNA peak (ORF or ORE); and c) RNA
114 peaks nearby (±1 kb) DNA peaks (PXP) (Fig 1C, Fig S1a-c, Table 1b).
115
116 We found that most of the CLAMP RNA peaks identified (71.4% in males and 89.5% in females)
117 are either proximal to (~1 kb) or overlapping with CLAMP-DNA peaks (Fig 1D). It is important
118 to note that the number of CLAMP-RNA peaks identified (Fig 1D) is greater than the number of
119 RNA targets (Fig. 1B) since many targets have multiple CLAMP-binding sites (Table 1b).
120 Notably, almost 50% of these proximal or overlapping peaks were actually within 250 bp of the
121 middle of the nearest CLAMP DNA peak in both male and female cells, indicated by enrichment
122 of CLAMP-RNA peaks near CLAMP-DNA peaks (Fig. 1C, E). These data suggest that CLAMP
123 links RNA to DNA during co-transcriptional splicing at a subset of its target genes (Table 1c) that
124 we have identified in early embryos and cell lines [15]. Notably, only a subset of CLAMP-dependent

125 spliced genes in the embryo and cell lines are direct CLAMP-RNA targets, revealing the context-
126 specificity of this function. These observations reveal that CLAMP directly contacts DNA and
127 RNA at a subset of its target genes, where it regulates splicing, indicating a direct, context-specific
128 function in co-transcriptional splicing.
129
130
131 **The CLAMP prion-like domain (PrLD) is essential for CLAMP-RNA interaction.**
132
133 After determining that CLAMP binds RNA, we examined its domain structure to identify domains
134 that may be responsible for RNA binding. CLAMP lacks a canonical **R**NA **r**ecognition **m**otif[18].
135 However, CLAMP contains a prion-like domain (PrLD), a subclass of intrinsically disordered
136 domains (IDR) enriched in polar residues similar to those found in yeast prion proteins (Fig 1A).
137 Many RBPs and TFs contain PrLDs[19,20] that can promote RNA-binding and drive the formation
138 of phase-separated biomolecular condensates[21]. Some PrLDs in TFs promote co-assembly with
139 RBPs to regulate transcription[22–24]. However, the mechanisms by which the PrLD regions within
140 TFs regulate alternative splicing remained unknown. Therefore, we expressed and purified full-
141 length CLAMP protein ($CLAMP^{WT}$-FL) and a CLAMP protein lacking the PrLD domain
142 ($CLAMP^{delPrLD}$-FL) (Fig 2A). We also generated the CLAMP 1-300 aa fragment, which removes
143 the mapped DNA binding domain but includes the PrLD domain (154-300 aa). Next, we
144 demonstrated the disordered nature of this domain (Fig 2B) using NMR spectroscopy. We also
145 generated an NMR spectrum of a mixture of total yeast RNA extract and isolated CLAMP PrLD
146 and found that CLAMP PrLD directly interacts with RNA (Fig 1C). Overall, we showed that the
147 CLAMP 1-300 aa region is sufficient for direct interaction with RNA.
148
149 Next, we further defined the role of the PrLD domain in promoting CLAMP-RNA interactions by
150 performing RNA-Protein EMSA assays using specific RNA probes targeting a well-studied
151 candidate RNA identified as a CLAMP interactor by iCLIP (Fig 2D). CLAMP is associated with
152 the Male Sex-lethal Complex (MSL), which regulates dosage compensation in males and contains
153 the *roX* (RNA on the X) long non-coding RNAs[13,25]. However, it was not known whether CLAMP
154 directly interacts with the *roX* RNAs. Because the *roX* RNAs have a defined structure and
155 function[26], we used *roX2,* identified by iCLIP as an *in vivo* male-specific CLAMP interactor (Table

156 1a), to determine whether CLAMP directly interacts with RNA *in vitro*. Therefore, we used a full-
157 length *roX2* probe (411 nt) for RNA-Protein EMSA gel shift assays (Fig 2D) with full-length
158 $CLAMP^{WT}$ and $CLAMP^{delPrLD}$ proteins that were expressed and purified from *E. coli*. At the same
159 protein and RNA concentrations, the $CLAMP^{delPrLD}$ protein binds to RNA less efficiently than
160 $CLAMP^{WT}$ (Fig 2E). Therefore, the CLAMP PrLD region promotes the binding of CLAMP to
161 RNA.
162
163 Next, we wanted to test how RNA sequence and known secondary structure regulate the CLAMP-
164 RNA interaction. In our iCLIP experiments, we identified the CLAMP-binding region on the *roX2*
165 RNA (23nt, Fig 2D). This region is just 12 nt downstream of a functionally important stem-loop
166 structure (Fig 2D), which is essential for *roX2* interaction with RNA helicase A, a component of
167 both the MSL complex and the spliceosome[26,27]. Therefore, we hypothesized that the *roX2* stem
168 loop, known to be functionally important, promotes the interaction between roX2 RNA and
169 CLAMP. Hence, we used two additional *roX2* RNA probes, which either completely delete both
170 the stem-loop and the CLAMP binding region (*roX2*-RNA^{mut}) or delete only the CLAMP binding
171 region identified by iCLIP (*roX2*-$RNA^{delCLAMP\ binding}$) (Fig 2D) for CLAMP-RNA Gel-shift assays.
172
173 We found that: 1) the *roX2* probe (342nt) lacking both the stem-loop and the iCLIP CLAMP
174 binding region (69nt) reduced CLAMP binding to the *roX2* RNA (Fig 1F); 2) In contrast, the *roX2*
175 $RNA^{delCLAMP\ binding}$ probe (399nt) lacking only the iCLIP CLAMP binding region (25nt) but
176 retaining the stem-loop, did not qualitatively affect CLAMP binding to the *roX2* RNA *in vitro* (Fig
177 S2). Therefore, the presence of the *roX2* RNA stem-loop and the CLAMP PrLD increases the
178 ability of CLAMP to directly interact with RNA.
179
180
181 **The CLAMP PrLD domain is important for CLAMP-dependent sex-specific splicing.**
182
183 Next, we tested whether regions of CLAMP that interact with RNA *in vitro* function *in vivo* to
184 regulate alternative splicing. We defined the role of the CLAMP PrLD by generating complete
185 (CLAMP Δ154-290 aa) and partial (CLAMP Δ160-290 aa) PrLD deleted mutant fly lines at the
186 endogenous CLAMP locus using CRISPR/Cas9 genomic mutagenesis and homologous repair[39]

187 (Fig 3A). Complete deletion of the PrLD (*clamp*^{delPrLD}) results in embryonic lethality. In contrast,
188 homozygous partial deletion (*clamp*$^{delPrLD+6Q}$) mutants that retain a stretch of 6 glutamines survive
189 to adulthood, suggesting that these glutamines (aa154-160) are essential for viability (Fig 3A).
190 Therefore, we assayed sex-specific alternative splicing in trans-heterozygous mutants
191 (*clamp*^{delPrLD}/*clamp*$^{\mathrm{delPrLD+6Q}}$) to ensure viability until it is possible to define the sex of animals at
192 the larval stage (Fig 3A, B). Analysis of RNA sequencing data using the time2splice pipeline[14]
193 from trans-heterozygous mutants (*clamp*^{delPrLD}/*clamp*$^{delPrLD+6Q}$) identifies CLAMP PrLD-
194 dependent female- and male-specific splicing (Fig 3B, Table 2a-c). More than 70% of the CLAMP
195 PrLD domain-dependent alternative splicing was sex-specific, with ~40-50% identified as new
196 cryptic splicing events that do not occur in wild-type larvae (Fig 3B). Therefore, the CLAMP PrLD
197 is essential for viability and impacts sex-specific alternative splicing.
198
199 To determine whether the CLAMP PrLD regulates sex-specific alternative splicing of RNAs that
200 are directly bound by CLAMP (Table 2a, b), we compared the RNAs bound to CLAMP *in vivo,*
201 identified by iCLIP (Table 1a), with CLAMP PrLD-dependent sex-specifically spliced genes
202 (Table 2a, b). Due to the large number of samples required, performing iCLIP in mutant L3 larvae
203 was not possible; therefore, we used cell line iCLIP targets. We determined that 14 CLAMP PrLD-
204 dependent sex-specifically spliced genes are direct CLAMP RNA interactors, identifying a smaller
205 subset of key genes for further analysis (Table 3). Moreover, most of these 14 direct targets are
206 themselves regulators of alternative splicing (Table 3). Therefore, it is possible that CLAMP,
207 which is heavily maternally deposited[28] and regulates splicing of 60% of all sex-specific spliced
208 isoforms[15], functions as an essential upstream splicing regulator by directly regulating the splicing
209 of genes encoding splicing factors, which then regulates alternative splicing of additional target
210 genes.
211
212 As an example of how CLAMP regulates a specific target gene involved in alternative splicing,
213 we investigated its function relative to Hrp38, a functional orthologue of hnRNPA2B1[29–31]. Hrp38
214 is a strong candidate for further study because we identified it as a physical and functional
215 interactor at the DNA, RNA, and protein levels[10] as described below. The *hrp38* transcript is one
216 of the 14 CLAMP PrLD-dependent spliced genes that are direct CLAMP RNA targets (Table 2a,
217 3). Integrating iCLIP with alternative splicing analysis suggested that in males, CLAMP binds to

218 exon1 of the *hrp38* transcript on chromatin, in which the *hrp38* transcript undergoes splicing to
219 remove exon2 (Fig 3C, D). Moreover, CLAMP binds both DNA and RNA at the *hrp38* gene locus
220 (Fig 3C). As described above, CLAMP-RNA gel shift assays and NMR studies (Fig 2) indicate
221 thatthe CLAMP PrLD domain is important for CLAMP-RNA binding. Therefore, we hypothesize
222 that in the CLAMP *PrLD* mutant males, the mutant CLAMP protein will not bind at exon1 of the
223 *hrp38* transcript with the same efficiency as the wildtype CLAMP (Fig 3D), which will affect
224 splicing between exon 1 and 4, resulting in a new spliced *hrp38* RNA variant.
225
226 To test the hypothesis, we first asked whether CLAMP regulates alternative splicing at the *hrp38*
227 locus. We found that in $clamp^{\mathrm{delPrLD}}/clamp^{\mathrm{delPrLD+6Q}}$ mutants, splicing of intron
228 AF:r6:3R:28600568:28600718:+ between exon2 and exon4 (Fig 3D) is regulated by CLAMP as
229 predicted by genome-wide splicing analysis (Table 2a). In contrast, in $clamp^{delPrLD}/clamp^{delPrLD+6Q}$
230 mutants, the *hrp38* transcript retains exon2 (Fig 3E, F). Next, we validated that the alternative
231 splicing of the *hrp38* gene is sex-specifically regulated by the CLAMP PrLD domain *in vivo* during
232 development at the third instar larval stage in males and females. In female and male mutants,
233 splicing of intron AF:r6:3R:28600568:28600718:+ occurs. However, in males, splicing was more
234 efficient than in females (Fig 3F). Our *in vivo* splicing analysis thus demonstrates that the CLAMP
235 PrLD domain is important for alternative splicing of *hrp38* during male and female development.
236
237 Since our iCLIP data show that CLAMP binds to exon1 of *hrp38* RNA, we compared $\mathrm{CLAMP}^{\mathrm{WT}}$
238 binding to *hrp38* exon1 and exon2 probes using RNA EMSAs and found that at the same protein
239 and RNA concentrations, CLAMP binds strongly to *hrp38* exon1 RNA with no unbound RNA
240 remaining (Fig 3G). Furthermore, the PrLD domain of CLAMP is important for CLAMP-*hrp38*
241 RNA binding (Fig 3H). Interestingly, $\mathrm{CLAMP}^{\mathrm{WT}}$ still binds to *hrp38* exon2 *in vitro* even though it
242 does not bind *in vivo,* suggesting that other RBPs modulate the specificity of CLAMP-RNA
243 interactions *in vivo*. Therefore, our *in vivo* and *in vitro* approaches demonstrate that CLAMP binds
244 to both DNA and RNA at the *hrp38* locus differentially in males and females and define how
245 CLAMP directly regulates the sex-specific splicing of the *hrp38* transcript.
246
247 Previously, we have demonstrated using proteomics that CLAMP sex-specifically interacts with
248 the Hrp38 protein[10], a component of highly mobile nuclear splicing speckles that regulate

249 alternative splicing[29,32–34]. Therefore, due to the functional interaction between CLAMP and Hrp38
250 at both the DNA, RNA, and protein levels, we determined how CLAMP regulates the sex-specific
251 dynamics of Hrp38, one of CLAMP's essential target genes and interactors, to define how CLAMP
252 regulates sex-specific splicing beyond directly interacting with the RNA of target genes.
253
254
255 **CLAMP regulates the nuclear dynamics of the alternative splicing regulator hnRNPA2/B1**
256 **orthologue Hrp38**
257
258 PrLD domains can drive the phase separation of proteins[21] and promote the formation of
259 subnuclear bio-condensates involved in transcription[22,35] and splicing[21,36]. Recent advances show
260 that biophysical properties of biomolecular condensates regulate splicing function[37]. Therefore,
261 we performed biochemical phase-separation assays to determine how the CLAMP PrLD regulates
262 CLAMP phase separation (Fig 4A). We found that the CLAMP PrLD contributes to phase
263 separation of the N-terminal half of CLAMP (residues 1-300). Many RBPs involved in splicing
264 form splicing condensates, and TFs form transcription condensates, but the mechanisms by which
265 transcription and splicing condensates interact to promote the fidelity of co-transcriptional splicing
266 remain very poorly understood[38]. Although the PrLDs of TFs can promote co-assembly of
267 biomolecular condensates with RBPs6,22,40, current work does not yet explain how TF-RBP
268 interactions regulate the dynamics of splicing condensates, which are linked to their function[37,39].
269
270 The hnRNPA1/B2 orthologue Hrp38 is a strong candidate to function with CLAMP to promote
271 alternative splicing because it is associated with CLAMP in three ways: 1) CLAMP interacts with
272 the *hrp38* RNA transcript in our iCLIP experiments (Table 1a); 2) CLAMP regulates alternative
273 splicing of the *hrp38* transcript (Table 2, Fig 3), and 3) CLAMP interacts with the Hrp38 protein
274 sex-specifically[10]. Hrp38 forms dynamic nuclear splicing condensates or speckles[29,32–34].
275 Therefore, we hypothesized that CLAMP PrLD-mediated phase separation affects the dynamics
276 of Hrp38 condensates. We tested our hypothesis by combining *in vitro* and *in vivo* approaches to
277 measure condensate formation, stability, and dynamics.
278

279 In *vitro*, CLAMP 1-300^{WT} and Hrp38 co-phase-separate into liquid-like condensates (Fig 4B). To
280 complement *in vitro* studies, we performed *in vivo* analysis of Hrp38 nuclear speckles in fixed and
281 live conditions in *Drosophila* third instar larval tissue (Fig 4C). Salivary gland (SG) and
282 malpighian tubule (MT) tissue nuclei were used since they have large polyploid or polytene nuclei,
283 making it easier to visualize and track nuclear speckles. Prior studies[40–43] suggest that larger
284 aggregates of hnRNPs are more immobile and have decreased function in regulating alternative
285 splicing. Therefore, we performed the following experiments in males and females to test our
286 hypothesis that the CLAMP PrLD domain regulates the dynamics of Hrp38 to drive changes in
287 sex-specific splicing: 1) We analyzed fixed SG nuclei expressing Hrp38-GFP samples to
288 determine the effect of the CLAMP PrLD domain on Hrp38 nuclear speckle size (Fig 4C-F); 2)
289 We performed live imaging to define how the CLAMP PrLD domain regulates the mobility of
290 Hrp38-GFP nuclear speckles (Fig 4C, G); 3) We performed FRAP analysis in MT nuclei to
291 measure the mobility of the Hrp38 protein in the nucleus by measuring the fraction of Hrp38 that
292 remains bound (Fig 4C, H). We also analyzed the co-localization of CLAMP and Hrp38 *in vivo*
293 (Fig. 4I-J) to determine how frequently they interact, and compared these findings with our in vitro
294 interaction results (Fig. 4B).
295
296 Compared with wild-type controls, in *clamp*^{delPrLD} mutants, we observe larger Hrp38 speckles (Fig.
297 4D-F) with lower mobility (Figs. 4G, H). The Hrp38 protein forms nuclear speckles (Fig 4D),
298 which are highly dynamic (Movie 1); however, in clampdelPrLD/clampdelPrLD+6Q mutants,
299 Hrp38 forms larger nuclear aggregates in both females and males compared to controls (Fig 4E),
300 with median speckle size in males slightly higher than in females (Figure 4F). Hrp38 nuclear size
301 negatively correlated with speckle dynamics (Fig 4G, H, Movie 2). FRAP analysis shows that in
302 *clamp*^{delPrLD}/*clamp*$^{delPrLD+6Q}$ mutant male and female individuals, Hrp38 remains more immobile
303 compared with matched wild-type controls (Fig 4G, Movie 3,4). Therefore, the presence of the
304 CLAMP PrLD domain reduces the size and increases the dynamics of the Hrp38 speckles.
305
306 Next, we analyzed the trajectories of moving Hrp38 speckles over time with live image analysis
307 (Materials and Methods) to determine whether CLAMP regulates their mobility. More restricted
308 tracks denote more immobile speckles, while more dispersed tracks represent more mobile
309 speckles[44]. Interestingly, we found that in wild-type controls, female Hrp38 speckles are less

310 mobile than male Hrp38 speckles. Without the CLAMP PrLD domain, Hrp38 speckles in males
311 become less mobile (Fig 4H), therefore becoming more similar to those in females. Therefore, the
312 CLAMP PrLD regulates the dynamics of Hrp38 speckles sex-specifically in live tissues, promoting
313 their enhanced mobility in males. We identified partial co-localization between CLAMP and
314 Hrp38, which is significantly increased in *clamp*^{delPrLD} mutant males (Fig. 4I- J). Therefore, the
315 CLAMP PrLD domain in males also prevents colocalization with Hrp38, supporting its differential
316 role in influencing Hrp38 dynamics in males and females.
317
318 Thus, the presence of the CLAMP PrLD reduces the size of Hrp38 splicing condensates, which
319 has been shown to increase their ability to mediate alternative splicing with high fidelity[45,46]
320 Therefore, our data support a model in which the CLAMP PrLD modulates Hrp38 condensates'
321 ability to regulate alternative splicing. Furthermore, the CLAMP PrLD promotes the formation of
322 CLAMP liquid droplets (Fig 4A), which can co-localize with Hrp38 splicing condensates (Fig.
323 4B). Deletion of CLAMP PrLD inhibits CLAMP phase separation *in vitro* (Fig 4A) and sex-
324 specifically regulates the dynamics of Hrp38 speckles *in vivo* (Fig. 4G- H). Overall, our data
325 suggest that the CLAMP PrLD sex-specifically alters the dynamic properties of Hrp38, preventing
326 it from forming large aggregates, which have been demonstrated to be non-functional[45,46].
327
328 Our data show that the PrLD domain of CLAMP is important for its phase-separation properties
329 (Fig 4A) and regulates the dynamics of the Hrp38 condensate under cellular conditions (Fig. 4D-
330 H). In vitro data also support the idea that CLAMP and Hrp38 can coexist as phase-separating
331 condensates (Fig 4B). Interestingly, in females, where Hrp38 protein associates with CLAMP[10],
332 Hrp38 protein is less dynamic and more in bound form compared to males (Fig 4H). The PrLD
333 domain of CLAMP plays an important role in the male-specific dynamic physical properties of
334 Hrp38. In *clamp*^{delPrLD}/*clamp*$^{delPrLD+6Q}$ mutants, there is an increase in bound Hrp38 and slower
335 Hrp38 dynamics in males (Fig 4H). Since this is associated with enhanced CLAMP and Hrp38
336 protein co-localization *in vivo* in *clamp*^{delPrLD}/*clamp*$^{delPrLD+6Q}$ males, we propose a hypothesis that
337 CLAMP and Hrp38 association in females and a lack of the same in males, mediated by the PrLD
338 domain of CLAMP, results in a difference in Hrp38 dynamics between the two sexes (Fig 4H).
339 The effect this difference has on Hrp38 function and its regulation needs further investigation.
340 Currently, our working model highlights that an Intrinsically disordered Domain (IDR), such as

341 PrLD in CLAMP (TF), changes biophysical properties of partner proteins (RBPs), drives sex-
342 specific protein-protein (Fig. 4I-J) and protein-RNA association (Fig. 2E, 3H), resulting in sex-
343 specific splicing changes (Fig. 3B, E-F).
344
345
346 **Discussion**
347
348 Very little is understood about how alternative splicing is targeted to the right place at the right
349 time within a highly compacted genome to prevent the formation of cryptic splicing events that
350 contribute to disease[1]. We hypothesized that transcription factors that interact with RNA-binding
351 proteins would be strong candidates for targeting alternative splicing to the correct genomic
352 locations in a developmental context. To test our hypothesis, we examined the *Drosophila* CLAMP
353 TF as a model to reveal new mechanisms by which the hundreds of TFs interacting with RNA and
354 RNA-binding proteins regulate splicing, because it regulates a well-defined alternative splicing
355 process, sex-specific splicing[15], and we can integrate genetic, genomic, live imaging, biochemical,
356 and structural approaches.
357
358 CLAMP is a pioneer TF that interacts with the male-specific MSL complex to regulate *Drosophila*
359 dosage compensation. It is essential for MSL targeting to GA-rich chromatin entry sites (CES) on
360 chromatin, thus helping to target the MSL complex to the X chromosome. Interestingly, CES
361 evolved from intronic polypyrimidine tracts, suggesting a further link with splicing[47]. We found
362 that, mechanistically similar to its role in dosage compensation, where it recruits a
363 ribonucleoprotein complex containing the *roX* non-coding RNAs, CLAMP directly links RNA to
364 DNA at a subset of target genes where it regulates sex-specific splicing.
365 Because not all CLAMP-dependent sex-specific spliced genes are both direct CLAMP-RNA and
366 CLAMP-DNA targets, CLAMP regulates alternative splicing through multiple mechanisms that
367 may be regulated by the presence of MSL complex in males but not females. Interestingly,
368 CLAMP regulates the splicing of many RBPs that are components of alternative splicing
369 complexes, including *hrp38.* The alternatively spliced forms of these proteins can result in protein
370 isoforms with different functions. CLAMP-regulated alternate first (AF) alternative splicing of
371 *hrp38* transcript gives rise to two different protein isoforms (Fig 3). How these two Hrp38 protein

372 isoforms differ in their physical and functional properties and how they regulate sex-specific
373 splicing is an important direction for future work.
374
375 We define CLAMP-regulated RBP protein dynamics as an alternative mechanism by which
376 CLAMP regulates splicing. We show that the CLAMP PrLD domain is essential for determining
377 the size of Hrp38 protein condensates, which in turn regulates their function. We hypothesize that
378 CLAMP affects Hrp38 splicing speckles by regulating the biophysical phase separation properties
379 of Hrp38 condensates. Aggregates of human Hrp38 homologue (HnRNPA2B1) results in
380 disfunction and disease phenotype, indicating the right size of the phase separated condensates is
381 essential for its function[45,46]. We show that CLAMP PrLD domain is essential for the Hrp38
382 condensate size, its loss resulting in aggregation (Fig. 4D-F), loss of phase separation properties
383 and dynamics (Fig. 4G-H) of Hrp38 protein, and would ultimately affect its function. Our data
384 support a model in which the CLAMP PrLD domain differentially regulates CLAMP-Hrp38
385 interactions to regulate splicing condensate properties in males and females. We further propose
386 that the interaction of CLAMP with the MSL complex in males but not females promotes sex
387 differences in Hrp38 function. The following evidence supports this model: 1) Hrp38 mobility is
388 different between males and females (Fig 4J) as is the CLAMP-Hrp38 protein interaction which
389 we identified as female-enriched from proteomic analysis[10]; 2) Hrp38 splicing condensate mobility
390 is more dysregulated males than in females in *clamp PrLD* mutants (Fig 4J); 3) The colocalization
391 between CLAMP and Hrp38 is decreased in males versus females, potentially due to competition
392 from the CLAMP-MSL interaction (Fig. 4I- J). Overall, our data support a model in which
393 CLAMP sex-specifically regulates the dynamics of the hnRNP orthologue Hrp38.
394
395 Thus, one of the determinants of the sex-specificity of the CLAMP-dependent alternative splicing
396 is sex-dependent variability in Hrp38 condensate dynamics. CLAMP interacts with the Hrp38
397 protein differentially between sexes[10]. Also, the PrLD domain of CLAMP regulates Hrp38
398 condensates more strongly in males, predicting that the CLAMP PrLD domain is important for
399 these male-biased interactions. This might be due to CLAMP interacting with the MSL complex
400 in males, thereby inhibiting its interaction with other proteins, such as Hrp38. However, the
401 absence of this complex would make such associations possible. The biomolecular interactions by

402 which the PrLD domain of CLAMP regulates Hrp38, determining CLAMP-Hrp38 interactions
403 needs further study.
404
405 Another determinant of the sex-specificity of CLAMP-dependent alternative splicing is that
406 CLAMP has different RNA targets in males and females, with the PrLD domain again playing an
407 important role. We hypothesize that sex-specific CLAMP-RNA targets result from CLAMP
408 having different RBP interactors in males and females, especially closer to chromatin[10]. his might
409 result from differential interactions between CLAMP and different ribonucleoprotein complexes
410 such as the MSL complex (MSL proteins and *roX* RNA) or the spliceosomal complex (RBPs and
411 snRNAs) on chromatin. In the future, new techniques like RD-SPRITE[48] that identify the
412 distribution of different nuclear clusters of RNAs on chromatin, including splicing hubs, can be
413 used to determine the global as well as specific local roles of CLAMP in establishing site-specific
414 RNA splicing in male compared with female cells.
415
416 We found substantial new cryptic splicing events[1] occurring in the absence of CLAMP (Fig 3B),
417 which indicates that at most genomic sites, CLAMP acts as an inhibitor of cryptic alternative
418 splicing events. Thus, overall, our data support a model where sex-specific differences in
419 alternative splicing arise from differential TF-RNA and TF-RBP interactions (Figs. 1 and 4). We
420 show for the first time that an intrinsically disordered domain (IDR) like the PrLD domain of
421 CLAMP in a TF regulates alternative splicing by altering the dynamics of splicing condensates.
422 Also, our data suggest that TFs that bind to specific DNA motifs and have RNA binding properties
423 are strong candidates for understanding how specific alternative splicing events are regulated
424 context-specifically to drive normal development and prevent the onset of disease states.
425
426
427 **Methods:**
428
429 **Cell culture:** Kc and S2 cells were maintained at 25°C in Schneider's media supplemented with
430 10% Fetal Bovine Serum and 1.4X Antibiotic-Antimycotic (Thermofisher Scientific, USA). Cells
431 were passaged every three days to maintain an appropriate cell density.
432

433 **Fly stocks and husbandry:** *Drosophila melanogaster* fly stocks were maintained at 24°C on
434 standard corn flour sucrose media. Fly strains with complete (CLAMP Δ154-290a.a) and partial
435 (CLAMP Δ160-290a.a) PrLD deleted mutant fly lines using CRISPR/Cas9 genomic mutagenesis
436 and homologous repair[49]. We used the flyCRISPR Optimal Target Finder tool from the University
437 of Wisconsin to design a CRISPR target sequence for *clamp*^{delPrLD} and *clamp*$^{delPrLD+6Q39}$. We
438 cloned target sequence oligonucleotides (one gRNA) for *clamp*^{delPrLD}
439 (sense:5'CTTCGGGTACAACGCCAAAGCGAG3';antisense:3'CCCATGTTGCGGTTTCGCTC
440 -CAAA5') and two gRNAs for *clamp*$^{delPrLD+6Q}$ (sense: 5'CTTCG-
441 AATAGAATCGCCGCCCGCT3';antisense:3'CTTATCTTAGCGGCGGGCGACAAA5')and(se
442 nse:5'CTTC-GTTGTGGCTGCACAGACTGG3';antisense:3'CAACACCGACGTGTCTGACC-
443 CAAA5') into the pU6-BbsI-chiRNA plasmid (Addgene no. 45946), following the protocol
444 outlined on the flyCRISPR website. We validated the correct ligation of the *clamp* CRISPR target
445 sequence into the pU6-BbsI-chiRNA plasmid by Sanger sequencing using universal M13 primers.
446 For homologous repair, we used
447 ssODN15'ACATAAGCTTTAAGTGTGACGTATGTTCAGATATGTTCCCTCATTTGGCAC
448 TTCTTAATGCTCATAGAGAGGCGAGCAGTGGGTCTGGCCATCATCCTGTGAAAAAAC
449 GAAATTCCCAGCAGATGACCAAAT3' for *clamp*^{delPrLD}and ssODN2
450 5'CTTCTTAATGCTCATAAGCGGATGCATACAGACGGGGAACAGCAGCAACAACAGC
451 AACATAACGCCCAAGCTGGCGGTACAACGCCAAAGCGAGAGGCGAGCAGTGGGTCT
452 GGCCATCATCCTGTGAAAAAA3' for *clamp*$^{delPrLD+6Q}$.The commercial service, BestGene Inc.,
453 microinjected the validated pU6-BbsI-chiRNA plasmid containing the *clamp* target sequence into
454 germline-expressing Cas9 flies Bloomington stock #51324. Flies containing a single mutation
455 were returned balanced over the *Curly of Oster* (*CyO)* second chromosome balancer. From these
456 progenies, we identified the CRISPR/Cas9-generated mutations by PCR across the target region
457 (forward:5′-GATATGTTCCCTCATTTGGCAC-3′, reverse:5′-
458 CACTCCCATGCTTCACACAG-3′). We isolated two independent clamp alleles from this
459 validation: (1) y^1, w^{1118}; *clamp*^{delPrLD}/*CyO*; and (2) y^1, w^{1118}; *clamp*$^{delPrLD+6Q}$/*CyO.* These were
460 crossed to obtain male and female *clamp*$^{delPrLD+6Q}$/*clamp*^{delPrLD} genotypes. Crisper/Cas9 generated
461 fly mutants and fly strain y^1 w^{1118}; P{w[+mC] =PTT-GC} Hrb98DE[ZCL0588] expressing
462 Hrp38GFP (Bloomington #6822) were crossed to obtain *clamp*$^{delPrLD+6Q}$/*clamp*^{delPrLD}male and
463 female expressing GFP tagged Hrp38 protein.

464

465 **CUT&RUN in cell lines:** Cells were allowed to grow to confluency and harvested. An equal
466 number of cells for each category was suspended in wash buffer and subjected to the Cut&Run
467 assay according to Skene et al. 2018[50] using rabbit anti-CLAMP (5µg) to immunoprecipitate
468 CLAMP-bound DNA fragments from male (S2) and female (Kc) cell lines. Three replicates for
469 males and females were run, but one female sample was dropped during later stages due to
470 insufficient starting material. Rabbit IgG was used as a control for each male and female cell line
471 sample. 1ng CUT&RUN DNA was used to generate libraries using the Kapa Hyper prep kit
472 (Roche, USA) and SeqCapAdapter Kit A (Roche, USA). 14 PCR cycles were used to amplify the
473 libraries. AMPure XP beads (Beckman Coulter, USA) were used for library purification, and
474 fragment analysis was performed to check the library quality. Paired-end 2x25 bp Illumina Hi-seq
475 sequencing was performed.

476

477 **RNA-seq in third instar larvae (L3):** Total RNA was extracted from control (y^1 w^{1118};
478 *hrp38GFP*) and *clamp* mutant (*yw, clamp*$^{delPrLD+6Q}$/*clamp*^{delPrLD}; *hrp38GFP*) male and female third
479 instar larvae (3 each) using Trizol (Invitrogen, USA). Four replicates were in each category
480 prepared. Messenger RNA was purified from total RNA using poly-T oligo-attached magnetic
481 beads. After fragmentation, the first strand of cDNA was synthesized using random hexamer
482 primers, followed by the second cDNA synthesis. The library was ready after end repair, A-tailing,
483 adapter ligation, size selection, amplification, and purification, followed by paired-end RNA-
484 sequencing in Illumina Novaseq 6000. The sequencing data were run through a SUPPA-based
485 time2splice pipeline[15] to identify CLAMP-dependent sex-specific splicing events. Data is to be
486 submitted to the GEO repository.

487

488 **iCLIP:** Cells were allowed to grow to confluency, and UV crosslinked using 254 nm UV light in
489 Stratalinker 2400 on ice (Stratagene, USA). UV-treated cells were lysed to get different cellular
490 fractions (Cytoplasmic, Nucleoplasmic, and Chromatin) according to the Fr-iCLIP (fractionation-
491 iCLIP) protocol from Brugiolo et al 2017[51]. Chromatin and nucleoplasmic fractions were sonicated
492 with a Branson digital sonicator at 30% amplitude for 30 seconds (10 sec on, 20 sec off) to disrupt
493 DNA prior to IP. All three fractions were separately centrifuged at 20,000 xg for 5 min at 4°C.
494 Fractions were tested by Western blotting using RNApolI for the Chromatin Fraction and Actin

495 for the Cytoplasmic Fraction. Protein quantification for each fraction was done using the
496 manufacturer's protocol for Pierce 660 nm protein assay reagent (Thermo Scientific, USA). Each
497 Fraction was subjected to the iCLIP protocol as described in Huppertz et al. 2014[52] using the
498 rabbit-CLAMP antibody to immunoprecipitate bound RNAs extracted using proteinase K and
499 phenol: chloroform. Custom cDNA libraries were prepared according to Huppertz et al. 2014[52]
500 using distinct primers Rt1clip-Rt16clip for separate samples containing individual 4nt-barcode
501 sequences that allow multiplexing of samples. cDNA libraries for each sample were amplified
502 separately using 31 cycles of PCR, mixed later, and sequenced using standard Illumina protocols.
503 Heyl et al. 2020[53] methods using the Galaxy CLIP-Explorer were followed to preprocess, perform
504 quality control, post-process, and peak calling.
505
506
507 **Validation of hrp38 splicing using RT-PCR assay:** Total RNA was extracted from 5 third instar
508 larvae (L3) female and male embryos expressing $clamp^{delPrLD+6Q}/clamp^{delPrLD}$and y^{1}, w^{1118}.
509 Following the manufacturer's protocol, we reverse-transcribed one microgram of total RNA using
510 the SuperScript VILO cDNA Synthesis Kit (Life Technologies, USA). We amplified target
511 sequences by PCR using primers designed to span alternatively spliced junctions (FP-
512 5'AGAACGGCAACTCCAATGGC3' and RP-5'GCCAGTCTCCTTGTCAATGA3') and Quick
513 load Taq 2X Master mix (#M0271L, NEB, USA) according to the manufacturer's protocol (28
514 cycles). 10ul of PCR product of each replicate for each gene was loaded in separate wells in 2%
515 agarose gels and imaged using a ChemiDoc™ MP Imaging system (BioRad, USA). All replicates
516 for each gene were loaded on the same gel. The gel images were quantified using the densitometry
517 steps with the Fiji image analysis tool. Student's t-tests were performed to determine significant
518 differences between groups (two samples at a time). Three replicates for RT-PCR samples were
519 performed.
520
521 **CLAMP Protein Expression and Purification:** Vectors encoding maltose binding protein
522 (MBP)-tagged CLAMP 1-300 and MBP-tagged CLAMP 1-300 delPrLD were produced by
523 cloning into the pTHMT vector. Plasmids were transformed into BL21 Star (DE3) cells, and
524 bacterial cultures were grown in a minimal M9 medium supplemented with ^{15}N ammonium
525 chloride. Cultures were grown at 37°C and 200 RPM to an optical density of 0.6-0.8 and

526 subsequently induced with 1 mM isopropyl-β-D-1-thiogalactopyranoside (IPTG) for 4 hours at
527 37°C. Cell pellets were harvested by centrifugation at 6,000 RPM, resuspended in lysis buffer (20
528 mM Tris pH 8, 1 M NaCl, 10 mM Imidazole, 1 mM DTT, and one EDTA-free protease inhibitor
529 tablet (Roche) per liter of culture), and lysed by sonication. The lysed cell suspension was cleared
530 by centrifugation at 20,000 RPM for 50 min. The supernatant was filtered using a 0.2 μm syringe
531 filter and loaded onto a HisTrap HP 5 ml column. The HisTrap column was first washed with 20
532 mM Tris pH 8, 1 M NaCl, 10 mM Imidazole, 1 mM DTT Buffer, and then the bound protein was
533 eluted with 20 mM Tris pH 8, 1 M NaCl, 500 mM Imidazole, 1 mM DTT buffer. Fractions
534 containing MBP-CLAMP 1-300 were collected and purified on a Superdex 200 (26/600) column
535 equilibrated in 20 mM Tris pH 8, 1.0 M NaCl buffer. As above, CLAMP PrLD (154-290) was
536 expressed and purified using HisTrap HP. Following that, CLAMP PrLD was collected from the
537 HisTrap HP, concentrated to 1 mL, and cleaved overnight with TEV protease to separate CLAMP
538 PrLD from the MBP in 20 mM Tris pH 8, 1 M NaCl, 10 mM Imidazole, and 1 mM DTT Buffer.
539 The cleaved protein was separated from the HisTag by a subtraction step, in which the cleaved
540 protein was flowed over the HisTrap HP column using the same Tris buffer previously described,
541 and the flow-through was collected. MBP-tagged Full-Length CLAMP was grown following the
542 same methods above. Once the Full-Length CLAMP cell lysate supernatant was loaded onto the
543 HisTrap HP 5 ml column, the protein was eluted with a gradient from 10 to 500 mM imidazole in
544 20 mM MES at pH 5.5 and 361 mM $CaCl_2$. Fractions containing MBP-CLAMP FL were collected
545 and purified on a Superdex 200 (26/600) column equilibrated in pH 5.5, 20 mM MES, and 361
546 mM CaCl2 buffer. For each CLAMP construct, fractions containing the desired protein were
547 verified by SDS-PAGE, concentrated using a 10 kDa centrifugation filter (Millipore), aliquoted,
548 and flash-frozen in liquid nitrogen.
549
550 **Hrp38 protein purification and phase separation assay:** Maltose-binding protein (MBP)-
551 tagged Hrp38 was expressed in BL21 Star (DE3) *E. coli* cells. The cells were resuspended in 20
552 mM NaPi at pH 7.4 with 300 mM NaCl and 10 mM imidazole, and the lysate was cleared by
553 centrifuging at 20,000 rpm for 60 mins at 4 °C. The supernatant was filtered using 0.2 μM filters
554 and loaded on a 5 ml HisTrap HP column. The protein was eluted using an imidazole gradient of
555 10-300 mM over 5-column volumes. The protein fractions were pooled and loaded on a Superdex
556 200 (26/600) column for size exclusion. 20 mM NaPi with 300 mM NaCl at pH 7.4 was used for

557 size exclusion chromatography and storage. Protein was flash frozen as aliquots of 1 mM.
558 Fluorescent labeling of the CLAMP 1-300 was done using AlexaFluor 488 maleimide dye, while
559 Hrp38 was labeled using 555 maleimide. The protein was diluted to 100 µM in 20 mM Tris buffer
560 at pH 7.4 with 50 mM NaCl, and a 5-fold concentration (500 µM) of the dye dissolved in DMSO
561 was added to 5% of the total volume. The reaction mixture was incubated for 1 hour, and then,
562 unbound AlexaFluor was removed using 1 ml Zeba spin desalting columns. The proteins were
563 concentrated to 1 mM, flash frozen, and stored. For phase separation and microscopy, Hrp38 was
564 buffer-exchanged into 20 mM Tris buffer at pH 7.4 containing 50 mM NaCl to a final
565 concentration of 20 µM. Stock and sample concentrations were measured using a NanoDrop
566 spectrophotometer with extinction coefficients of 130,000 M^{-1} cm^{-1} for Hrp38 and 78270 for MBP
567 CLAMP 1-300. 1 µM of AlexaFluor-labeled CLAMP was added to Hrp38, and TEV protease was
568 added to cleave the MBP tag. Less than 1% fluorescent protein was used in all samples. A Nikon
569 spinning-disc confocal microscope (Nikon Eclipse Ti2) was used for imaging at 20X
570 magnification with 1.5X zoom. The images were processed using ImageJ.
571
572 **NMR Sample Preparation and Spectroscopy:** ^{15}N isotopically labeled samples of CLAMP 1-
573 300 were prepared at 50 µM in a buffer containing 20 mM MES pH 5.5, 100 mM NaCl, 1 mM
574 DTT, and 5% D_2O, and then moved into a 5 mm NMR tube using a glass pipette. CLAMP
575 concentration was determined by measuring absorbance at 280 nm (and then dividing absorbance
576 by the extinction coefficient estimated by the Expasy ProtParam). NMR spectra were recorded ona
577 Bruker Avance 850 MHz ^{1}H Larmor frequency spectrometer with HCN TCI z-gradient
578 cryoprobes. A two-dimensional $^{1}H^{15}N$ HSQC was acquired using spectral widths of 10.5 ppm and
579 30.0 ppm in the direct and indirect dimensions, with 3072 and 512 total points and acquisition
580 times of 172 ms and 99.0 ms, respectively. Samples of isotopically labeled CLAMP PrLD were
581 prepared at 20 µM in a buffer containing 50 mM MES, pH 5, and 5% D_2O. Because the PrLD
582 domain of CLAMP contains no tyrosines or tryptophans, the A_{280} absorbance could not be
583 measured to determine the protein concentration. Instead, sample concentration was estimated by
584 measuring absorbance at 230 nm and calculating the extinction coefficient to be 300 M-1 cm-1 per
585 peptide bond (40.5 mM-1 cm-1 for CLAMP PrLD). Torula yeast was added to one PrLD sample
586 at a 1:1 Protein to RNA ratio by weight, and NMR spectra were acquired in 5 mm NMR tubes on
587 a Bruker Avance 850 MHz ^{1}H Larmor frequency spectrometer. Both 1H15N HSQC spectra were

588 acquired with spectral widths of 14.0 ppm and 25.0 ppm in the direct and indirect dimensions,
589 respectively, with 2048 and 256 total points and acquisition times of 86.0 ms and 59.4 ms,
590 respectively. All data were processed and analyzed using NMRPipe and CCPNMR Analysis 2.5
591 software[54,55].
592
593 **RNA Electrophoretic Mobility Shift Assays:** *rox2*RNA probes at 100 nM and *hrp38* RNA
594 probes at 50nM were incubated with MBP-tagged FL CLAMP^{WT} protein or MBP-tagged FL
595 CLAMP^{delPrLD} protein in REMSA binding buffer provided with the LightShift Chemiluminescent
596 RNA EMSA kit (Thermo Scientific, USA) at room temperature for 30 min according to the
597 manufacturer's protocol. Reactions were loaded onto 6% TBE retardation gels (Thermo Fisher
598 Scientific) and run in 0.5× Tris–borate–EDTA buffer for one hour. RNA-Protein complex was
599 transferred to the Nylon membrane using the iBlot transfer system (ThermoFisher Scientific), and
600 the probe signal was detected using a Chemiluminescent Nucleic acid detection module (#80880,
601 ThermoFisher Scientific).
602
603 **Immunostaining of *Drosophila* tissue**:
604 Third instar larval salivary gland tissue from control and *clamp*$^{delPrLD+6Q}$/*clamp*^{delPrLD} male and
605 female dissected in 1XPBS (Phosphate Buffer Saline, 10X PBS, Boston Bioproducts Inc, USA)
606 and fixed in 4% PFA in 1XPBS (Paraformaldehyde, Sigma Aldrich, USA) for 20 min. Incubated
607 in 1% PBST (Triton-X in 1XPBS) for 10 minutes and washed twice in 0.1% PBST for 10 minutes
608 each. They were incubated in a moist chamber with a blocking solution (3% BSA, bovine serum
609 albumin in 0.1%PBST) for 2 hours at RT. Tissues were then incubated in rabbit anti-CLAMP
610 (1:500, SDIX) overnight at 4 degrees Celsius in a blocking solution in a moist chamber. Washed
611 tissues in 0.1% PBST three times for 15 minutes each. Secondary anti-rabbit Alexa fluor 568 at
612 1:200 dilution was used to incubate tissue for 2 hrs at RT in a blocking solution in a moist chamber
613 and again, washed in 0.1% PBST three times for 15 minutes each, followed by DAPI staining
614 (1ug/ml in 1XPBS) for 10 min at RT in the dark. After two washes in 0.1% PBST for 10 min each,
615 tissues were mounted on a slide in Vectashield (Vector Laboratories Inc, USA).
616
617
618

619 **Fluorescence recovery after photobleaching (FRAP)**:
620 *In vivo* (Malphighian tubule principal cell nucleus expressing Hrp38GFP in control and
621 *clamp*$^{delPrLD+6Q}$/*clamp*^{delPrLD}male and female third instar larvae) FRAP was performed on a Nikon
622 Spin-disc Confocal Microscope with a 488 nm laser on a 60× objective,taking frames without
623 delay (short time course and fast-recovering control) with 3-sec acquisition pre-bleaching,
624 bleaching using 473 nm laser at 100%, and 2-minute acquisition post-bleach. Malpighian tubules
625 (MTs) were dissected in Grace's Insect media with a 1:50 dilution of ProlongLive (antifading
626 agent). A 6% slurry of low-melting agarose (A9414-5G) in Grace's Insect media was used to
627 stabilize the MTs during imaging on a bridge slide with a cavity to pour the agarose, which was
628 allowed to solidify, forming a soft base to mount the tissue. The intensities recorded in selected
629 regions of interest were obtained using NIS-Elements software. Data fitting and immobile fraction
630 analysis were performed using the NIS-Elements software FRAP analysis module.
631
632 ***In-vivo* live imaging:** Salivary gland expressing Hrp38GFP (nuclear) in control and
633 *clamp*$^{delPrLD+6Q}$/*clamp*^{delPrLD} male and female third instar larvae were dissected in Grace's Insect
634 media with a 1:50 dilution of ProlongLive (antifading agent) and mounted in the dissecting media
635 on a bridge slide with low-melting agarose (A9414-5G) in Grace's Insect media as a base. Moving
636 Hrp38GFP condensates in the nucleus were imaged using a 488 nm laser on a Nikon Spinning
637 Disc Confocal Microscope at 60X magnification for 2 minutes each, without any delay in
638 acquisition.
639
640
641 **Computational Methods**
642 **CUT&RUN Data analysis:** Sequenced reads were run through FASTQC[56](fastqc
643 replicate_R1_001.fastq.gz replicate_R2_001.fastq.gz) with default parameters to check the quality
644 of raw sequence data and filter out any sequences flagged for poor quality. Sequences were
645 trimmed and reassessed for quality using TrimGalore
646 (https://github.com/FelixKrueger/TrimGalore/issues/25) and FastQC[56], respectively. All Illumina
647 lanes of the same flow cell. fastq files were merged, and sequenced reads were mapped to the
648 release 6 *Drosophila melanogaster* genome (dm6). We compared Bowtie2[57], HISAT2[58], and
649 BWA[59]. We found the best alignment quality with BWA and thus used its results downstream.

Next, we performed conversion to BAM and sorting (e.g., using: bowtie2 -x dm6_genome -1 replicate_R1_001.fastq.gz -2 replicate_R2_001.fastq.gz -S out. sam> stout.txt 2> alignment_info.txt; samtools view -bSout.sam>out.bam; rm -rfout.sam; samtools sort out.bam -o out.sorted.bam). We removed reads (using samtools) with a MAPQ less than 30 and any PCR duplicates (identified using Picard MarkDuplicates 2.20.2). Peaks identified using MACS2[60](macs2 callpeak -t out.sorted.bam -B -f BAM --nomodel --SPMR --keep-dup all -g dm --trackline -n outname --cutoff-analysis --call-summits -p 0.01 --outdiroutdir) and keep duplicates separate**.** To calculate fold-enrichment, macs2 is rerun (macs2 bdgcmp -t $treat -c $control -o $out.sorted.bam_FE.bdg -m FE 2> $ out.sorted.bam_FE.log; macs2 bdgcmp -t $treat -c $control -o $out.sorted.bam_logLR.bdg -m logLR -p 0.00001 2). For motif analysis, the MEME[61] suite was used. Data was submitted to the GEO repository (#GSE174781, #GSE220981, and #GSE220053).

iCLIP Data analysis: The method from Heyl et al. 2020[53] using the Galaxy CLIP-Explorer was followed to preprocess, perform quality control, post-process, and perform peak calling. UMI tools were used for preprocessing, and then UMI tools and Cutadapt were used for Adapter, Barcode, and UMI removal. Cutadapt (Galaxy version 3.5) was used for filtering with a custom adaptersequenceAGATCGGAAGAGCGGTTCAGCAGGAATGCCGAGACCGATCTCGTATGCCGTCTTCTGCTTG. All other settings followed the Heyl et al. 2020 Galaxy iCLIP-explorer workflow. UMI-Tools Extract (Galaxy Version 1.1.2+galaxy2) was then used with a barcode pattern of NNNXXXXNN. No unpaired reads were allowed. The barcode was on the 3' end. Je-Demultiplex (Galaxy Version 1.2.1) was then used for demultiplexing. FastQC was used for quality control. Mapping was done by RNA STAR (Galaxy version 2.5.2b-2) using dm6. All settings were chosen based on the existing parameters from the iCLIP-explorer settings. We selected FALSE for the option to use end-to-end read alignments with no soft-clipping. bedtools used for Read-Filtering, and UMI-Tools (Galaxy version 0.5.3.0) for de-duplication. PEAKachu was used for Peak Calling to generate bed files. The PEAKachu settings were followed using the Galaxy CLIP-explorer workflow. The maximum insert size was set to 150, the minimum cluster expression fraction was set to 0.01, the minimum block overlap was set to 0.5, and the minimum block expression was set to 0.1. The Mad Multiplier was set to 0.0, the Fold Change Threshold was set to 2.0, and the adjusted p-value threshold was set to 0.05. Peaks were annotated using RCAS[62] (RNA Centric Annotation System), an R package using RStudio. MEME Suite is used

681 for motif detection. RCAS was used to analyze the functional features of transcriptomes isolated
682 by iCLIP. Data was submitted to the GEO repository (#GSE205987).
683
684 **Integrating CUT&RUN and iCLIP data:** A Python script was created that iterates through all
685 of the DNA peak bed files for CLAMP DNA binding sites in Kc and S2 cell lines (CUT&RUN
686 data, #GSE220053) as a reference and tests for overlap with CLAMP-bound RNA peaks (each
687 sequence is between 25-50bp in size) in the Kc and S2 (iCLIP data, (#GSE205987). The overlaps
688 are categorized into four main categories based upon the location of the overlap: 1) completely
689 overlapping (purple lines in frequency plot), 2) partially overlapping at the DNA peak start site
690 (red lines in frequency plot); 3) partially overlapping at the DNA peak end site (blue lines in
691 frequency plot) and 4) non-overlapping, i.e. when there is an overlap in a region outside the DNA
692 binding site (yellow lines in frequency plot). This extended region is defined by the *scope* variable
693 in the script, allowing the overlap to look for binding sites near the DNA binding site (this scope
694 is 2 kb, including the DNA binding site). We note that multiple RNA peaks can be found within a
695 single DNA peak. These overlaps are placed onto a [-scope, scope] region. Then, each type of
696 overlap, shown in a different color, is overlaid and plotted on a frequency plot. So, if the frequency
697 at a given base pair is 5, five overlaps contain that base pair within the region defined by the scope.
698
699 **Analysis of Imaging data:**
700

701 ***In vivo* co-localization of CLAMP and Hrp38.** Images of the fixed salivary glands
702 immunostained for CLAMP (magenta, anti-CLAMP antibody) and Hrp38 (green, GFP) were
703 acquired as z-stacks and saved as nd2 files. The raw image data from each nd2 file was converted
704 to 3D numpy arrays for each specified channel (magenta and green) employing the nd2 reader
705 Python package. Colocalization analysis was then performed to determine the Pearson Correlation
706 Coefficient (PCC) and corresponding p-value between the two channels of each nd2 file using the
707 scikit-image Python package (scikit-image 0.22.0), indicating the degree of overlap between the
708 proteins (CLAMP and Hrp38). The PCC and p-value were obtained for 20 male controls, 38 male
709 $clamp^{delPrLD+6Q}/clamp^{delPrLD}$, 22 female controls, and 28 female $clamp^{delPrLD+6Q}/clamp^{delPrLD}$ nd2
710 files. The mean PCC and standard error of the mean (calculated using SciPy) for each background

711 across all nd2 files were then plotted using the matplotlib Python package. Statistical analysis was
712 performed to compare colocalization coefficients across different experimental conditions,
713 including pairwise p-values and t-values for each experimental background relative to the others.

714 All image processing and analysis for colocalization were done through a custom Python script.
715 (https://github.com/smritivaidyanathan/3D_Speckle_Volume_Quantifier/blob/main/scripts/coloc
716 alizer.py).

717

718 **Quantification of speckle dynamics; Bound Fraction calculations** Live-imaging movies (2 min
719 long) of dynamically moving GFP-tagged Hrp38 protein were pre-processed using Fiji (ImageJ)
720 Python macro script, involving Fiji Plugins and built-in software on the Hrp38 condensate (green
721 channel) to distinguish Hrp38 phase condensates from the cell background. Simple Ratio bleach
722 correction was applied, and the minimum and maximum intensity adjustment was executed based
723 on the mean intensity and standard deviation of intensity. The specific adjustment method varied
724 depending on the image quality, ensuring optimal visibility of Hrp38 condensate speckles.
725 Afterward, background subtraction was performed with a rolling ball radius of 120 pixels. The
726 conversion to a binary image involved max entropy thresholding, although the minimum
727 thresholding method was employed for some images to accommodate diverse lighting conditions.
728 The thresholder images were saved as TIFF files for use in the TrackIt tracking software[44], a
729 program for tracking and analyzing single-molecule experiments developed by the Gebhardt lab.
730 In total, 29 male control movies, 55 male $clamp^{delPrLD+6Q}/clamp^{delPrLD}$ mutant movies, 23 female
731 control movies, and 65 female $clamp^{delPrLD+6Q}/clamp^{delPrLD}$ mutant movies were utilized in
732 subsequent analyses.

733

734 For tracking analysis, TIFF movies from each experimental condition were loaded into TrackIt[44],
735 and analysis was performed using MATLAB on a Windows 10 PC, utilizing default settings with
736 specific parameter adjustments: threshold (4), tracking radius (8), minimum track length (2), one
737 gap frame allowed, and minimum track length before the gap (3). Each experimental condition
738 was analyzed using TrackIt's MATLAB-based data visualization tool, with settings further edited
739 for formatting in a MATLAB script. Tracking data outputs were used for bound fraction analysis
740 according to the TrackIt package[44]. TrackIt provided information on tracked events, including

741 long, short, linked, and non-linked events. The calculation of bound fractions by TrackIt involved
742 determining the ratio of the sum of short and long events to non-linked events. Movie-wise bound
743 fraction values and the pooled fraction were plotted (sum over all movies for each type of event).
744 Statistical analysis comparing the bound fraction of Hrp38 speckles across different experimental
745 conditions was performed using a paired Student's t-test for each experimental background against
746 the others. Error bars for the pooled fraction values were calculated using linear error propagation,
747 following the formula indicated in the TrackIt Manual[44] (https://gitlab.com/GebhardtLab/TrackIt/-
748 /blob/master/TrackIt_manual.pdf?ref_type=heads).

749 **Quantification of speckles volume** Z-stack confocal images from fixed third instar salivary gland
750 tissue of male and female wildtype control and $clamp^{delPrLD+6Q}/clamp^{delPrLD}$ mutant samples
751 expressing GFP tagged Hrp38 protein in the nucleus were used to determine the size of Hrp38
752 nuclear speckles in the presence of $CLAMP^{WT}$ and $CLAMP^{delPrLD}$. We wrote a Python script for
753 the pre-processing step to create a binary image, with all areas covered by a fluorescently tagged
754 Hrp38 condensate to be represented by a 1, and all others to be marked as 0, using the following
755 steps: a. Conversion of the z-stacks to a 3D array using the nd2reader Python package. b.
756 Smoothing the image to reduce noise using a Gaussian filter with a sigma value of 1.0. c.
757 Thresholding the image using the formula, where the threshold was calculated as follows:

758 Each pixel in the smoothed image is represented by an intensity value ranging from 0 (black) to
759 255 (white). Following the application of a smoothing algorithm, the arithmetic average (μ) and
760 standard deviation (σ) are calculated across all pixel intensities in the smoothed image.

761 Thresholding was performed to generate a binary image using these calculated parameters. The
762 threshold value (T) is defined as:

763 $T = \mu + (n \times \sigma)$

764 where n is a user-defined constant, with $n \geq 0$, for each pixel in the smoothed image, if the intensity
765 was greater than T, the corresponding pixel in the binary image was assigned a value of 1 (white).
766 Conversely, if the intensity was less than or equal to T, the corresponding pixel in the binary image
767 was assigned a value of 0 (black). The resulting binary image retained the same dimensions and
768 pixel count as the original smoothed image.

769 d. Storing and sending to the next step of the pipeline. In the above function, the value of n varied
770 between datasets. It was refined through a visual inspection of the thresholded 3D image using the
771 Napari Viewer python package (https://napari.org), and n was set to equal to 7. In total, 17 male
772 control, 15 male *clamp*$^{delPrLD+6Q}$/*clamp*^{delPrLD} mutant, 17 female control, and 25 female
773 *clamp*$^{delPrLD+6Q}$/*clamp*^{delPrLD} mutant z-stack movies were processed and analyzed. To account for
774 irregular shapes of speckles, the segmentation algorithm union-find[63] with modified connectivity
775 parameter set as None, meaning that the program will not limit the number of jumps, set to
776 input.ndim, or the size of the array itself (Skimage. measure, 2024) was used. The mean speckle
777 size for each category was plotted with the 95% confidence intervals, calculated using a Z-score
778 of 1.96. The same was done for medians, except using bootstrapping with 1000 samples to
779 calculate the error bars, again calculated using a Z-score of 1.96. The pairwise p-values and t-
780 values were calculated using an independent sample t-test (student t-test). Details of the 3D volume
781 quantification scripts can be found on the Github page:
782 https://github.com/smritivaidyanathan/3D_Speckle_Volume_Quantifier.

783

784 **Competing Interest Statement**

785 The authors declare no competing interests.

786

787 **Acknowledgments**

788 This work was supported by R35GM126994 to E.N.L. from NIH, and by National Science
789 Foundation (Directorate for Biological Sciences) 1845734 and R01GM147677 to N.L.F. A.M.C
790 is funded by the NSF Graduate Research Fellowship and CCMB, Brown University. We thank
791 Bloomington Stock Center for fly lines. We thank Steve Henikoff for the pAMNase protein and
792 spike-in DNA for Cut and Run.

793

794 **Author Contributions**

795 **M.R**., **N. L. F,** and **E.N.L**. planned experiments, analyzed results, and wrote the manuscript. **J.Z**
796 did all protein purifications and the NMR and phase separation assays for CLAMP. **M.R.**
797 conducted the experimental work and collected data for Cut and Run, iCLIP, FRAP, Live imaging,
798 RNA-EMSA, RNA isolation for RNA-sequencing, and generated fly mutants. **P.M** analyzed third

instar larval RNA-seq data using the time2splice pipeline to identify CLAMP-dependent splicing events, integrated CLAMP iCLIP data with CLAMP CUT&RUN in cell lines, and performed the splicing assay for *hrp38*. **S.V.** analyzed all the imaging data sets. **R.V.** performed the co-LLPS assay with Hrp38 and CLAMP. **J.S** cloned CLAMP1-300 and CLAMP1-300del PrLD clones. **J.S.**, **V.C., I.P.,** and **K.C.** helped with RNA-EMSA assays. **A.H.** analyzed the iCLIP-seq data. **A.M.C** analyzed CUT&RUN data. **S.H.W.** helped with NMR analysis. **V.J.** and **N.W.** helped with CLAMP Protein Expression and Purification. **A.E.C** and **R.P** helped with the protein and NMR assay.

References

1. Aldalaqan, S., Dalgliesh, C., Luzzi, S., Siachisumo, C., Reynard, L.N., Ehrmann, I., and Elliott, D.J. (2021). Cryptic splicing: common pathological mechanisms involved in male infertility and neuronal diseases. Cell Cycle *21*, 219–227.

2. Boumpas, P., Merabet, S., and Carnesecchi, J. (2023). Integrating transcription and splicing into cell fate: transcription factors on the block. Wiley Interdiscip. Rev. RNA *14*, e1752.

3. Han, H., Braunschweig, U., Gonatopoulos-Pournatzis, T., Weatheritt, R.J., Hirsch, C.L., Ha, K.C.H., Radovani, E., Nabeel-Shah, S., Sterne-Weiler, T., and Wang, J. (2017). Multilayered control of alternative splicing regulatory networks by transcription factors. Mol. Cell *65*, 539–553. e7.

4. Saulnier, O., Guedri-Idjouadiene, K., Aynaud, M.-M., Chakraborty, A., Bruyr, J., Pineau, J., O'grady, T., Mirabeau, O., Grossetête, S., and Galvan, B. (2021). ERG transcription factors have a splicing regulatory function involving RBFOX2 that is altered in the EWS-FLI1 oncogenic fusion. Nucleic Acids Res. *49*, 5038–5056.

5. Jabre, I., Reddy, A.S.N., Kalyna, M., Chaudhary, S., Khokhar, W., Byrne, L.J., Wilson, C.M., and Syed, N.H. (2019). Does co-transcriptional regulation of alternative splicing mediate plant stress responses? Nucleic Acids Res. *47*, 2716–2726.

6. Oksuz, O., Henninger, J.E., Warneford-Thomson, R., Zheng, M.M., Erb, H., Vancura, A., Overholt, K.J., Hawken, S.W., Banani, S.F., and Lauman, R. (2023). Transcription factors interact with RNA to regulate genes. Mol. Cell *83*, 2449–2463. e13.

7. He, C., Sidoli, S., Warneford-Thomson, R., Tatomer, D.C., Wilusz, J.E., Garcia, B.A., and Bonasio, R. (2016). High-resolution mapping of RNA-binding regions in the nuclear proteome of embryonic stem cells. Mol. Cell *64*, 416–430.

8. Cassiday, L.A., and Maher, L.J., III (2002). Having it both ways: transcription factors that bind DNA and RNA. Nucleic Acids Res. *30*, 4118–4126.

835 9. Göös, H., Kinnunen, M., Salokas, K., Tan, Z., Liu, X., Yadav, L., Zhang, Q., Wei, G.-H., and
836 Varjosalo, M. (2022). Human transcription factor protein interaction networks. Nat. Commun. *13*,
837 766.

838 10. Urban, J.A., Urban, J.M., Kuzu, G., and Larschan, E.N. (2017). The Drosophila CLAMP protein
839 associates with diverse proteins on chromatin. PLoS One *12*, e0189772.

840 11. Kuzu, G., Kaye, E.G., Chery, J., Siggers, T., Yang, L., Dobson, J.R., Boor, S., Bliss, J., Liu, W.,
841 Jogl, G., et al. (2016). Expansion of GA dinucleotide repeats increases the density of CLAMP
842 binding sites on the X-chromosome to promote Drosophila dosage compensation. PLoS Genet. *12*,
843 e1006120.

844 12. Kaye, E.G., Booker, M., Kurland, J.V., Conicella, A.E., Fawzi, N.L., Bulyk, M.L., Tolstorukov,
845 M.Y., and Larschan, E. (2018). Differential occupancy of two GA-binding proteins promotes
846 targeting of the Drosophila dosage compensation complex to the male X chromosome. Cell Rep. *22*,
847 3227–3239.

848 13. Soruco, M.M.L., Chery, J., Bishop, E.P., Siggers, T., Tolstorukov, M.Y., Leydon, A.R., Sugden,
849 A.U., Goebel, K., Feng, J., Xia, P., et al. (2013). The CLAMP protein links the MSL complex to the
850 X chromosome during Drosophila dosage compensation. Genes Dev. *27*, 1551–1556.

851 14. Albig, C., Tikhonova, E., Krause, S., Maksimenko, O., Regnard, C., and Becker, P.B. (2019). Factor
852 cooperation for chromosome discrimination in Drosophila. Nucleic Acids Res. *47*, 1706–1724.

853 15. Ray, M., Conard, A.M., Urban, J., Mahableshwarkar, P., Aguilera, J., Huang, A., Vaidyanathan, S.,
854 and Larschan, E. (2023). Sex-specific splicing occurs genome-wide during early \textitDrosophila
855 embryogenesis. Elife *12*, e87865.

856 16. Straub, T., Zabel, A., Gilfillan, G.D., Feller, C., and Becker, P.B. (2013). Different chromatin
857 interfaces of the Drosophila dosage compensation complex revealed by high-shear ChIP-seq.
858 Genome Res. *23*, 473–485.

859 17. Alekseyenko, A.A., Peng, S., Larschan, E., Gorchakov, A.A., Lee, O.-K., Kharchenko, P., McGrath,
860 S.D., Wang, C.I., Mardis, E.R., Park, P.J., et al. (2008). A sequence motif within chromatin entry
861 sites directs MSL establishment on the Drosophila X chromosome. Cell *134*, 599–609.

862 18. Pomeranz-Krummel, D., and Nagai, K. (2001). RNA-Binding Domains in Proteins. In Encyclopedia
863 of Genetics, S. Brenner and J. H. Miller, eds. (Academic Press), pp. 1733–1735.

864 19. March, Z.M., King, O.D., and Shorter, J. (2016). Prion-like domains as epigenetic regulators,
865 scaffolds for subcellular organization, and drivers of neurodegenerative disease. Brain Res. *1647*, 9–
866 18.

867 20. Harrison, A.F., and Shorter, J. (2017). RNA-binding proteins with prion-like domains in health and
868 disease. Biochem. J *474*, 1417–1438.

869 21. Gotor, N.L., Armaos, A., Calloni, G., Torrent Burgas, M., Vabulas, R.M., De Groot, N.S., and
870 Tartaglia, G.G. (2020). RNA-binding and prion domains: the Yin and Yang of phase separation.
871 Nucleic Acids Res. *48*, 9491–9504.

872 22. Wang, Y., Zolotarev, N., Yang, C.-Y., Rambold, A., Mittler, G., and Grosschedl, R. (2020). A prion-
873 like domain in transcription factor EBF1 promotes phase separation and enables B cell programming

874 of progenitor chromatin. Immunity *53*, 1151–1167.e6.

875 23. Yang, J., Xu, H., Zhang, C., Yang, X., Cai, W., and Chen, X. (2023). A prion-like domain of TFEB
876 mediates the co-aggregation of TFEB and mHTT. Autophagy *19*, 544–550.

877 24. Brodsky, S., Jana, T., and Barkai, N. (2021). Order through disorder: The role of intrinsically
878 disordered regions in transcription factor binding specificity. Curr. Opin. Struct. Biol. *71*, 110–115.

879 25. Eggers, N., Gkountromichos, F., Krause, S., Campos-Sparr, A., and Becker, P.B. (2023). Physical
880 interaction between MSL2 and CLAMP assures direct cooperativity and prevents competition at
881 composite binding sites. Nucleic Acids Res. *51*, 9039–9054.

882 26. Ilik, I.A., Maticzka, D., Georgiev, P., Gutierrez, N.M., Backofen, R., and Akhtar, A. (2017). A
883 mutually exclusive stem–loop arrangement in roX2 RNA is essential for X-chromosome regulation
884 in Drosophila. Genes Dev. *31*, 1973–1987.

885 27. Park, Y., Oh, H., Meller, V.H., and Kuroda, M.I. (2005). Variable splicing of non-coding roX2
886 RNAs influences targeting of MSL dosage compensation complexes in Drosophila. RNA Biol. *2*,
887 157–164.

888 28. Duan, J., Rieder, L., Colonnetta, M.M., Huang, A., Mckenney, M., Watters, S., Deshpande, G.,
889 Jordan, W., Fawzi, N., and Larschan, E. (2021). CLAMP and Zelda function together to promote
890 Drosophila zygotic genome activation. Elife *10*. https://doi.org/10.7554/eLife.69937.

891 29. Borah, S., Wong, A.C., and Steitz, J.A. (2009). Drosophila hnRNP A1 homologs Hrp36/Hrp38
892 enhance U2-type versus U12-type splicing to regulate alternative splicing of the prospero twintron.
893 Proc. Natl. Acad. Sci. U. S. A. *106*, 2577–2582.

894 30. Li, S., Zhang, P., Freibaum, B.D., Kim, N.C., Kolaitis, R.-M., Molliex, A., Kanagaraj, A.P., Yabe, I.,
895 Tanino, M., and Tanaka, S. (2016). Genetic interaction of hnRNPA2B1 and DNAJB6 in a
896 Drosophila model of multisystem proteinopathy. Hum. Mol. Genet. *25*, 936–950.

897 31. Kim, H.J., Kim, N.C., Wang, Y.-D., Scarborough, E.A., Moore, J., Diaz, Z., MacLea, K.S.,
898 Freibaum, B., Li, S., and Molliex, A. (2013). Mutations in prion-like domains in hnRNPA2B1 and
899 hnRNPA1 cause multisystem proteinopathy and ALS. Nature *495*, 467–473.

900 32. Blanchette, M., Green, R.E., MacArthur, S., Brooks, A.N., Brenner, S.E., Eisen, M.B., and Rio, D.C.
901 (2009). Genome-wide analysis of alternative pre-mRNA splicing and RNA-binding specificities of
902 the Drosophila hnRNP A/B family members. Mol. Cell *33*, 438–449.

903 33. Herold, N., Will, C.L., Wolf, E., Kastner, B., Urlaub, H., and Lührmann, R. (2009). Conservation of
904 the protein composition and electron microscopy structure of Drosophila melanogaster and human
905 spliceosomal complexes. Mol. Cell. Biol. *29*, 281–301.

906 34. Singh, A.K., and Lakhotia, S.C. (2015). Dynamics of hnRNPs and omega speckles in normal and
907 heat shocked live cell nuclei of Drosophila melanogaster. Chromosoma *124*, 367–383.

908 35. Mann, R., and Notani, D. (2023). Transcription factor condensates and signaling driven
909 transcription. Nucleus *14*, 2205758.

910 36. Hennig, S., Kong, G., Mannen, T., Sadowska, A., Kobelke, S., Blythe, A., Knott, G.J., Iyer, K.S.,
911 Ho, D., and Newcombe, E.A. (2015). Prion-like domains in RNA binding proteins are essential for
912 building subnuclear paraspeckles. J. Cell Biol. *210*, 529–539.

913 37. Giudice, J., and Jiang, H. (2024). Splicing regulation through biomolecular condensates and
914 membraneless organelles. Nat. Rev. Mol. Cell Biol. *25*, 683–700.

915 38. Guo, Y.E., Manteiga, J.C., Henninger, J.E., Sabari, B.R., Dall'Agnese, A., Hannett, N.M., Spille, J.-
916 H., Afeyan, L.K., Zamudio, A.V., and Shrinivas, K. (2019). Pol II phosphorylation regulates a
917 switch between transcriptional and splicing condensates. Nature *572*, 543–548.

918 39. Liu, S., Wang, T., Shi, Y., Bai, L., Wang, S., Guo, D., Zhang, Y., Qi, Y., Chen, C., Zhang, J., et al.
919 (2021). USP42 drives nuclear speckle mRNA splicing via directing dynamic phase separation to
920 promote tumorigenesis. Cell Death Differ. *28*, 2482–2498.

921 40. Forman-Kay, J.D., Ditlev, J.A., Nosella, M.L., and Lee, H.O. (2022). What are the distinguishing
922 features and size requirements of biomolecular condensates and their implications for RNA-
923 containing condensates? RNA *28*, 36–47.

924 41. Deshaies, J.-E., Shkreta, L., Moszczynski, A.J., Sidibé, H., Semmler, S., Fouillen, A., Bennett, E.R.,
925 Bekenstein, U., Destroismaisons, L., Toutant, J., et al. (2018). TDP-43 regulates the alternative
926 splicing of hnRNP A1 to yield an aggregation-prone variant in amyotrophic lateral sclerosis. Brain
927 *141*, 1320–1333.

928 42. Shin, Y., Berry, J., Pannucci, N., Haataja, M.P., Toettcher, J.E., and Brangwynne, C.P. (2017).
929 Spatiotemporal control of intracellular phase transitions using light-activated optoDroplets. Cell *168*,
930 159–171.e14.

931 43. Shin, Y., and Brangwynne, C.P. (2017). Liquid phase condensation in cell physiology and disease.
932 Science *357*, eaaf4382.

933 44. Kuhn, T., Hettich, J., Davtyan, R., and Gebhardt, J.C.M. (2021). Single molecule tracking and
934 analysis framework including theory-predicted parameter settings. Sci. Rep. *11*, 9465.

935 45. Ryan, V.H., Dignon, G.L., Zerze, G.H., Chabata, C.V., Silva, R., Conicella, A.E., Amaya, J., Burke,
936 K.A., Mittal, J., and Fawzi, N.L. (2018). Mechanistic view of hnRNPA2 low-complexity domain
937 structure, interactions, and phase separation altered by mutation and arginine methylation. Mol. Cell
938 *69*, 465–479.e7.

939 46. Martinez, F.J., Pratt, G.A., Van Nostrand, E.L., Batra, R., Huelga, S.C., Kapeli, K., Freese, P., Chun,
940 S.J., Ling, K., Gelboin-Burkhart, C., et al. (2016). Protein-RNA networks regulated by normal and
941 ALS-associated mutant HNRNPA2B1 in the nervous system. Neuron *92*, 780–795.

942 47. Quinn, J.J., Zhang, Q.C., Georgiev, P., Ilik, I.A., Akhtar, A., and Chang, H.Y. (2016). Rapid
943 evolutionary turnover underlies conserved lncRNA-genome interactions. Genes Dev. *30*, 191–207.

944 48. Quinodoz, S.A., Jachowicz, J.W., Bhat, P., Ollikainen, N., Banerjee, A.K., Goronzy, I.N., Blanco,
945 M.R., Chovanec, P., Chow, A., Markaki, Y., et al. (2021). RNA promotes the formation of spatial
946 compartments in the nucleus. Cell *184*, 5775–5790.e30.

947 49. Gratz, S.J., Rubinstein, C.D., Harrison, M.M., Wildonger, J., and O'Connor-Giles, K.M. (2015).
948 CRISPR-Cas9 genome editing in Drosophila. Curr. Protoc. Mol. Biol. *111*, 31.2.1–31.2.20.

949 50. Skene, P.J., Henikoff, J.G., and Henikoff, S. (2018). Targeted in situ genome-wide profiling with
950 high efficiency for low cell numbers. Nat. Protoc. *13*, 1006–1019.

951 51. Brugiolo, M., Botti, V., Liu, N., Müller-McNicoll, M., and Neugebauer, K.M. (2017). Fractionation

952 iCLIP detects persistent SR protein binding to conserved, retained introns in chromatin, nucleoplasm
953 and cytoplasm. Nucleic Acids Res. *45*, 10452–10465.

954 52. Huppertz, I., Attig, J., D'Ambrogio, A., Easton, L.E., Sibley, C.R., Sugimoto, Y., Tajnik, M., König,
955 J., and Ule, J. (2014). iCLIP: protein-RNA interactions at nucleotide resolution. Methods *65*, 274–
956 287.

957 53. Heyl, F., Maticzka, D., Uhl, M., and Backofen, R. (2020). Galaxy CLIP-Explorer: a web server for
958 CLIP-Seq data analysis. Gigascience *9*. https://doi.org/10.1093/gigascience/giaa108.

959 54. Delaglio, F., Grzesiek, S., Vuister, G.W., Zhu, G., Pfeifer, J., and Bax, A. (1995). NMRPipe: a
960 multidimensional spectral processing system based on UNIX pipes. J. Biomol. NMR *6*, 277–293.

961 55. Skinner, S.P., Fogh, R.H., Boucher, W., Ragan, T.J., Mureddu, L.G., and Vuister, G.W. (2016).
962 CcpNmr AnalysisAssign: a flexible platform for integrated NMR analysis. J. Biomol. NMR *66*, 111–
963 124.

964 56. Andrews, S. (2010). FastQC: a quality control tool for high throughput sequence data http://www.
965 bioinformatics. babraham. ac. uk/projects/fastqc. Babraham Bioinformatics.

966 57. Langmead, B., and Salzberg, S.L. (2012). Fast gapped-read alignment with Bowtie 2. Nat. Methods
967 *9*, 357–359.

968 58. Kim, D., Paggi, J.M., Park, C., Bennett, C., and Salzberg, S.L. (2019). Graph-based genome
969 alignment and genotyping with HISAT2 and HISAT-genotype. Nat. Biotechnol. *37*, 907–915.

970 59. Li, H., and Durbin, R. (2009). Fast and accurate short read alignment with Burrows-Wheeler
971 transform. Bioinformatics *25*, 1754–1760.

972 60. Zhang, Y., Liu, T., Meyer, C.A., Eeckhoute, J., Johnson, D.S., Bernstein, B.E., Nusbaum, C., Myers,
973 R.M., Brown, M., Li, W., et al. (2008). Model-based analysis of ChIP-Seq (MACS). Genome Biol.
974 *9*, R137.

975 61. Bailey, T.L., Johnson, J., Grant, C.E., and Noble, W.S. (2015). The MEME suite. Nucleic Acids Res.
976 *43*, W39–W49.

977 62. Uyar, B., Yusuf, D., Wurmus, R., Rajewsky, N., Ohler, U., and Akalin, A. (2017). RCAS: an RNA-
978 centric annotation system for transcriptome-wide regions of interest. Nucleic Acids Res. *45*, e91.

979 63. van der Walt, S., Schönberger, J.L., Nunez-Iglesias, J., Boulogne, F., Warner, J.D., Yager, N.,
980 Gouillart, E., Yu, T., and scikit-image contributors (2014). scikit-image: image processing in Python.
981 PeerJ *2*, e453.

982
983
984
985
986
987
988
989

990 **Figure legends**
991
992 **Figure 1**. **CLAMP is a dual DNA/RNA-binding protein with sex-specific RNA targets. A.**
993 Schematic showing the design of the fractionation iCLIP experiment to determine CLAMP RNA
994 targets in different nuclear fractions of male and female *Drosophila* cell lines. **B**. Venn diagrams
995 show the distribution of CLAMP RNA targets between male (S2) and female (Kc) cell types and
996 between chromatin (ChF) and nucleoplasm (NF) fractions (**four replicates** for each category
997 performed except **three replicates** for the Kc nucleoplasm fraction). The number within each
998 circle/overlap region denotes the number of RNA targets/genes, and the percentage of RNA
999 targets/gene is shown within the parentheses in each category. **C.** Frequency distribution of
1000 CLAMP RNA binding peaks represented as peak counts (right side secondary Y-axis) from iCLIP
1001 data (**four replicates** male and female chromatin fraction) plotted over a region (±1kb across the
1002 middle of the DNA peak) spanning CLAMP DNA binding peaks (black line, CUT&RUN data,
1003 **three replicates** for males, **two replicates** for females). Complete overlaps (CRO) are denoted by
1004 magenta, proximal (within ±1kb across the DNA peak),non-overlaps (PXP) in yellow, partial
1005 overlaps in red (near the starting boundary of DNA peaks, ORF), and blue (near the ending
1006 boundary of DNA peaks, ORE). **D-E.** Bar plots (**D**) and pie-chart (**E**) show the distribution of the
1007 number of CLAMP-RNA peaks that overlap with CLAMP-DNA peaks or are within a ±1kb region
1008 of CLAMP-DNA peaks (proximal peaks, PXP). Overlapping peaks are sub-categorized into
1009 complete RNA peaks overlapping with DNA peaks (CRO), overlapping RNA peaks with DNA
1010 peak front (5' end, ORF), and overlapping RNA peaks with DNA peak 3' end (ORE).
1011
1012
1013 **Figure 2**. **The PrLD domain of CLAMP is important for Clamp-RNA interaction A.**
1014 Schematic of full-length (FL) CLAMP depicting the location of the PrLD (residues 154-290 amino
1015 acids) and other essential features in the presence (left) and absence (right) of the PrLD **B.** The
1016 $^{1}H^{15}N$ HSQC spectrum of 1-300aa CLAMP at 50 μM demonstrates the largely disordered nature
1017 of the protein that lacks the DNA-binding domain. Dispersed resonances in the region from 7.9 –
1018 7.0 ppm in the ^{1}H and 115-122 ppm in the ^{15}N likely arise from the folded N-terminal zinc finger
1019 **C.** $^{1}H^{15}N$ HSQC spectra of CLAMP PrLD at 20 μM with (red) and without (blue) torula yeast
1020 RNA, showing changes consistent with binding. **D.** Schematic shows the length of *roX2* RNA

1021 probes used to study the role of RNA sequence/structure in CLAMP-RNA interaction with RNA
1022 gel shift assays (RNA-EMSA). **E.** RNA-EMSA showing the binding of increasing amounts of
1023 MBP fusion CLAMP-Full length and CLAMP PrLD domain deleted protein to *roX2* RNA
1024 biotinylated probes (100 nM). Concentrations (µM) of CLAMP protein increase from left to right.
1025 **F.** RNA-EMSA showing difference in binding of full-length (FL) CLAMP (fused to MBP) to
1026 *roX2-RNA* probe with (411nt) and without (342nt) stem-loop, and CLAMP-roX2 RNA binding
1027 region identified from iCLIP. Concentrations (µM) of CLAMP FL increase from left to right.
1028 Concentrations (µM) of CLAMP FL and CLAMPdel PrLD increase from left to right.
1029
1030 **Figure 3. The CLAMP PrLD domain regulates sex-specific splicing in *Drosophila* third instar**
1031 **larvae A.** Region of CLAMP-Full length protein was deleted to create fly mutants expressing full
1032 (*clamp*^{delPrLD}) and partial (*clamp*$^{delPrLD+6Q}$) PrLD deleted CLAMP protein using CRISPR-Cas
1033 genome editing. The schematic shows the corresponding stages until they survive, and, within
1034 parentheses, the male-to-female ratio in adults of those that survive. **B.** Pie chart showing the
1035 proportion of CLAMP PrLD domain-dependent alternative splicing events that are sex-specific in
1036 male and female third instar larvae. The number of splicing events is noted within parentheses. **C.**
1037 CLAMP-DNA binding (CUT&RUN data) and CLAMP-RNA binding in chromatin fraction
1038 (iCLIP data) peaks visualized in the IGV genome browser at the *hrp38* gene location in female
1039 (Kc cells, red) and male (S2 cells, blue). **D.** Schematic of *hrp38* transcript showing CLAMP
1040 binding at exon1 and alternative splicing of intron AF:r6:3R:28600568:28600718:+ in
1041 *clamp*^{delPrLD}/*clamp*$^{delPrLD+6Q}$ mutant male. **E-F.** The agarose electrophoretic gel image is shown in
1042 **E,** and the corresponding bar plot in **F** shows the change in levels of intron
1043 AF:r6:3R:28600568:28600718:+ spliced isoforms resulting from alternative splicing events in
1044 male and female L3 larvae under control *clamp*^{WT}(green) and *clamp*^{delPrLD}/*clamp*$^{delPrLD+6Q}$ (orange)
1045 conditions. The isoform transcript levels are normalized by the levels of the *gapdh* housekeeping
1046 gene transcript. p-values (paired Student's t-test) for groups showing significant differences are
1047 noted at the top of the line connecting the compared groups (**three replicates** for each category).
1048 **G-H.** RNA EMSA mobility shift showing a difference in the efficiency of CLAMP full-length
1049 protein-*hrp38* exon1 and exon2 binding (**G**) and that of CLAMP-PrLD domain deleted and
1050 CLAMP full-length protein with *hrp38* exon1(**H**). CLAMP^{delPrLD} and CLAMP^{WT}-Full length MBP

1051 fusions were used at increasing concentrations of 0, 3.1, 6.2, and 12.5 µM with 50 nM biotinylated
1052 RNA probes.
1053
1054 **Figure 4. The CLAMP PrLD domain regulates the dynamics of hnRNPA2 homolog Hrp38**
1055 **biomolecular condensates. A**. DIC micrograph of CLAMP 1-300 with or without PrLD domain
1056 (100 µM) at 150 mM salt concentration with 5% PEG. **B**. Single plane confocal images showing
1057 the co-phase separation of Alexa Fluor 488 maleimide dye-labeled Hrp38 with a single cysteine
1058 added for labeling (green) and Alexa Fluor 555 maleimide dye-labeled 1-300 CLAMP (pseudo
1059 color, magenta) under phase separating conditions for Hrp38. **C**. Schematic showing experimental
1060 design setup for studying Hrp38 nuclear condensates in vivo using fixed and live tissue imaging
1061 techniques. **D-F.** Confocal image of a single plane of third instar larval salivary gland nuclei
1062 expressing Hrp83-GFP in $clamp^{WT}$(green) and $clamp^{delPrLD}/clamp^{delPrLD+6Q}$ conditions in **D,** with
1063 bar plots showing mean (**E**) and median (**F**) Hrp38 speckle/condensate size in control and
1064 $clamp^{delPrLD}/clamp^{delPrLD+6Q}$ male and females. p-values (paired Student's t-test) for groups
1065 showing significant differences in mean speckle size are noted at the top of the line connecting the
1066 compared groups. **G**. Bar plots showing the percentage of Hrp38-GFP in the immobile phase
1067 (FRAP analysis) in male and female L3 larvae under control $clamp^{WT}$ and
1068 $clamp^{delPrLD}/clamp^{delPrLD+6Q}$ conditions. p-values (paired Student's t-test) for groups showing
1069 significant differences marked by an asterisk are noted at the top of the line connecting the
1070 compared groups—**n**=Number of Malpighian tubule principal cell nuclei, **N**= Number of
1071 individuals. **H**. Mean bound fraction of Hrp38GFP speckles (Number of Hrp38GFP speckles
1072 bound, i.e., immobile track lengths/the total number of Hrp38GFP speckles with all types of track
1073 lengths over a fixed time-period) from live imaging of salivary gland nuclei expressing Hrp38-
1074 GFP in male and female $clamp^{WT}$and $clamp^{delPrLD}/clamp^{delPrLD+6Q}$ individuals. Each dot **N**
1075 represents each individual (movie), and '**n**' denotes the number of Hrp38 speckles identified in
1076 each category. p-values (paired Student's t-test) for groups showing significant differences in the
1077 mean fraction of bound Hrp38 speckles are noted at the top of the line connecting the compared
1078 groups. **I-J.** Confocal single plane images of immune-stained third instar larval salivary gland
1079 nuclei showing in vivo partial co-localization of CLAMP (magenta) and Hrp38 (green) speckles
1080 in control and mutant ($clamp^{delPrLD}/clamp^{delPrLD+6Q}$) males in **I** with corresponding bar plots in **J**
1081 showing the Pearson's colocalization coefficient between CLAMP (magenta) and Hrp38 (green)

1082 in both males and females. p-values (paired Student's t-test) for groups showing significant
1083 differences are noted at the top of the line connecting the compared groups.
1084
1085
1086
1087 **Supplementary Figure legends**
1088
1089
1090 **Figure S1. A-C** IGV genome browser view showing relative CLAMP DNA and RNA binding at
1091 *mrj* (**A),** *sf3b3* **(B),** and *sqd* **(C)** genes.
1092
1093
1094 **Figure S2.** RNA-EMSA showing the binding of increasing amounts of MBP fusion CLAMP-Full
1095 length and CLAMP PrLD domain deleted protein to *roX2* RNA biotinylated probes without the
1096 CLAMP binding sequence. Concentrations (µM) of CLAMP protein increase from left to right.
1097 $CLAMP^{delPrLD}$ and $CLAMP^{WT}$-Full length MBP fusions were used at increasing concentrations of
1098 0, 3.1, 6.2, and 12.5 µM with 200 nM biotinylated RNA probes.
1099
1100
1101
1102 **Table legends**
1103
1104 **Table 1a:** CLAMP RNA targets identified in the nuclear fractions of male (S2) and female (Kc)
1105 cells.
1106
1107
1108 **Table 1b:** List of genes and genomic locations where CLAMP RNA peaks completely overlap
1109 with CLAMP DNA peaks (CRO), CLAMP RNA peaks overlap with 5' and 3' ends of DNA peaks
1110 (ORF and ORE), and CLAMP RNA peaks are proximal to DNA peaks (PXP) in male (S2) and
1111 female (Kc) cells.
1112
1113 **Table 2a:** List of all CLAMP PrLD-dependent differentially spliced genes in *Drosophila* third
1114 instar larvae (L3).
1115
1116 **Table 2b:** List of all CLAMP PrLD-dependent differentially sex-specifically spliced genes in
1117 *Drosophila* female third instar larvae (L3).

1118

1119 **Table 2c:** List all CLAMP PrLD-dependent differentially sex-specifically spliced genes in
1120 *Drosophila* male third instar larvae (L3).

1121

1122 **Table 3:** List of CLAMP PrLD-dependent male and female specifically spliced genes whose RNA
1123 isoforms are direct targets of the CLAMP protein.

1124

1125

1126

1127 **Movie legends**

1128

1129

1130 **Movie 1:** Live imaging of dynamic Hrp38GFP in the control male third instar larval salivary
1131 gland cell nucleus.

1132

1133 **Movie 2:** Live imaging of dynamic Hrp38GFP in *clamp*^{delPrLD}/*clamp*$^{delPrLD+6Q}$ male third instar
1134 larval salivary gland cell nucleus.

1135

1136 **Movie 3:** Show recovery of Hrp38GFP during FRAP experiment in the control (female) third
1137 instar larval Malpighian tubule cell nucleus.

1138

1139 **Movie 4:** Show recovery of Hrp38GFP during FRAP experiment in *clamp*^{delPrLD}/*clamp*$^{delPrLD+6Q}$
1140 (female) third instar larval Malpighian tubule cell nucleus.

1141

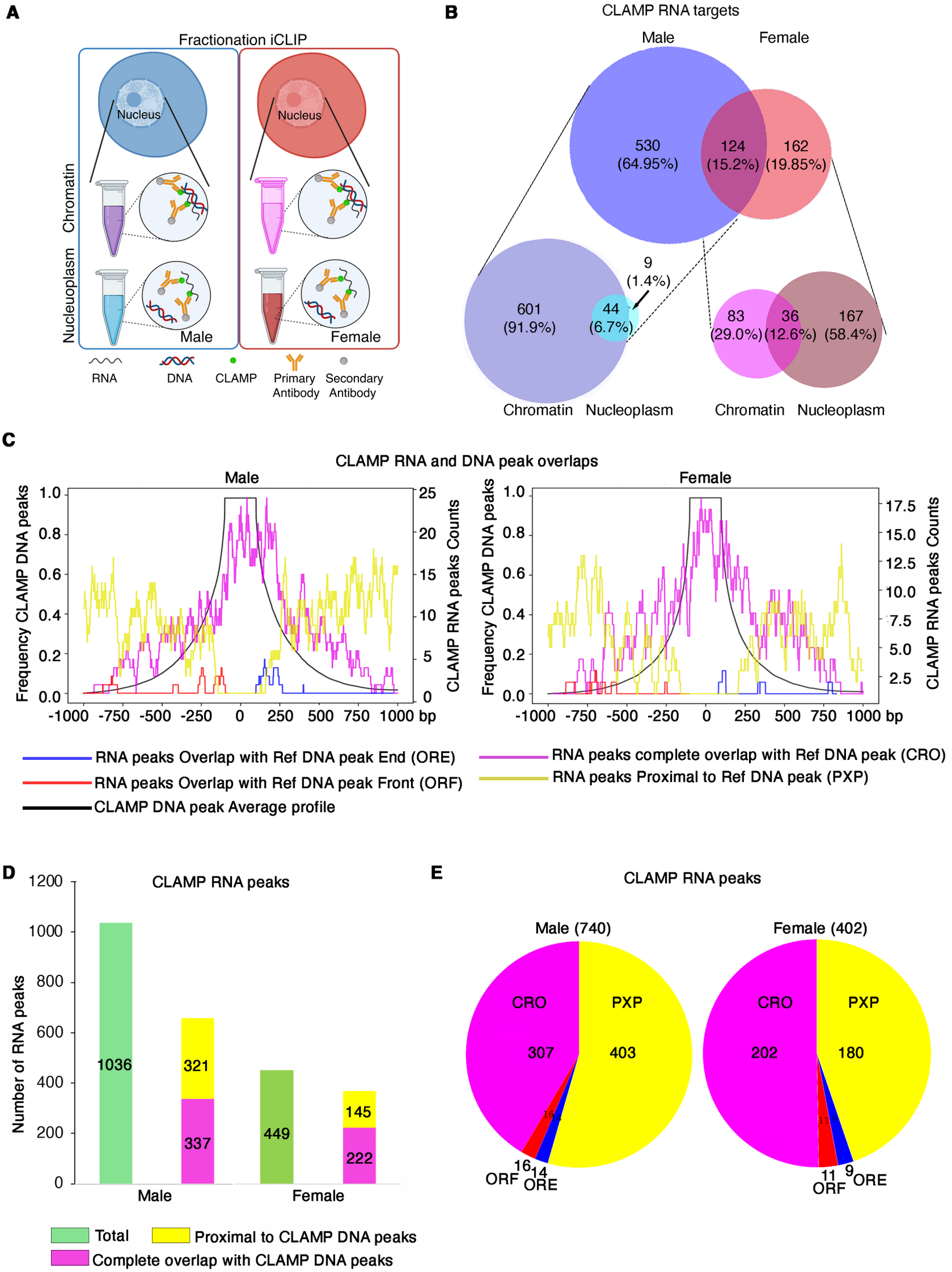
A
Fractionation iCLIP
Nucleus
Nucleus
Chromatin
Nucleuoplasm
Male
Female
RNA
DNA
CLAMP
Primary Antibody
Secondary Antibody
B
CLAMP RNA targets
Male
Female
530 (64.95%)
124 (15.2%)
162 (19.85%)
9 (1.4%)
601 (91.9%)
44 (6.7%)
83 (29.0%)
36 (12.6%)
167 (58.4%)
Chromatin
Nucleoplasm
Chromatin
Nucleoplasm
C
CLAMP RNA and DNA peak overlaps
Male
Female
Frequency CLAMP DNA peaks
CLAMP RNA peaks Counts
-1000 -750 -500 -250 0 250 500 750 1000 bp
RNA peaks Overlap with Ref DNA peak End (ORE)
RNA peaks Overlap with Ref DNA peak Front (ORF)
CLAMP DNA peak Average profile
RNA peaks complete overlap with Ref DNA peak (CRO)
RNA peaks Proximal to Ref DNA peak (PXP)
D
CLAMP RNA peaks
Number of RNA peaks
1036
321
337
449
145
222
Male
Female
Total
Proximal to CLAMP DNA peaks
Complete overlap with CLAMP DNA peaks
E
CLAMP RNA peaks
Male (740)
Female (402)
CRO
PXP
307
403
16
14
ORF
ORE
CRO
PXP
202
180
11
9
ORF
ORE

Figure 2 Ray, Zaborowsky et al 2026

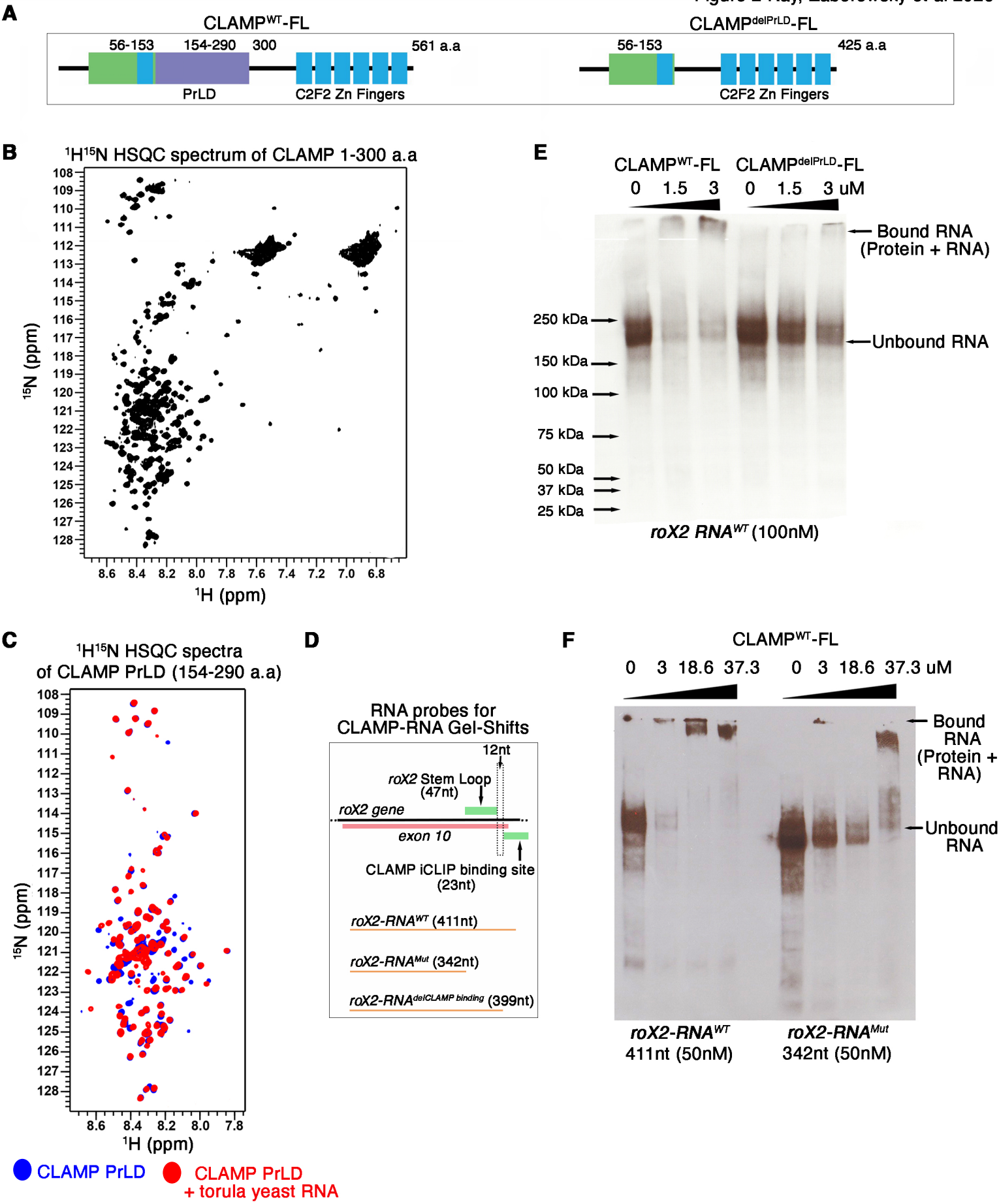

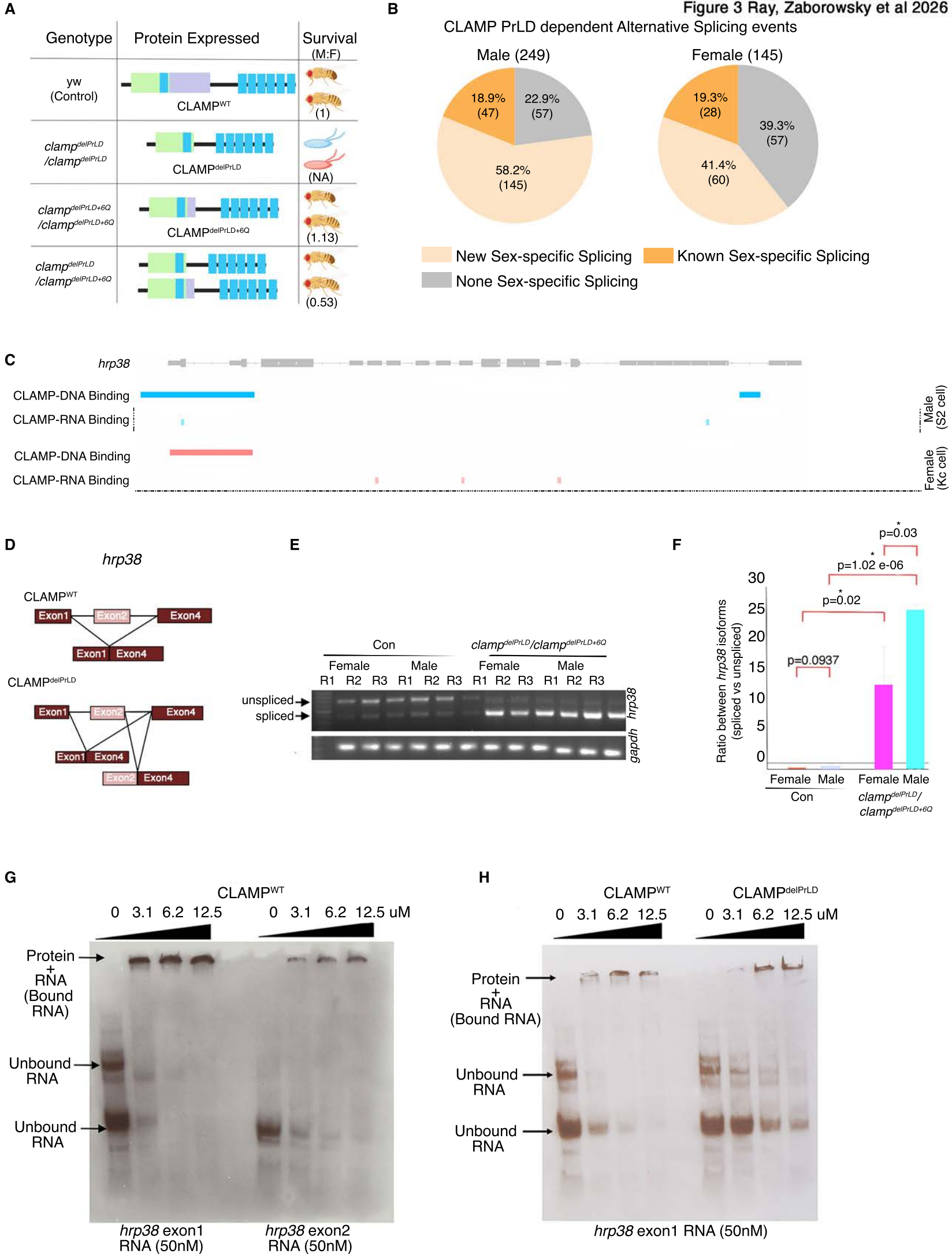
A
Genotype
Protein Expressed
Survival (M:F)
yw (Control)
CLAMP^WT
(1)
clamp^delPrLD /clamp^delPrLD
CLAMP^delPrLD
(NA)
clamp^delPrLD+6Q /clamp^delPrLD+6Q
CLAMP^delPrLD+6Q
(1.13)
clamp^delPrLD /clamp^delPrLD+6Q
(0.53)
B
CLAMP PrLD dependent Alternative Splicing events
Male (249)
18.9% (47)
22.9% (57)
58.2% (145)
Female (145)
19.3% (28)
39.3% (57)
41.4% (60)
New Sex-specific Splicing
Known Sex-specific Splicing
None Sex-specific Splicing
C
hrp38
CLAMP-DNA Binding
CLAMP-RNA Binding
Male (S2 cell)
CLAMP-DNA Binding
CLAMP-RNA Binding
Female (Kc cell)
D
hrp38
CLAMP^WT
Exon1
Exon2
Exon4
Exon1
Exon4
CLAMP^delPrLD
Exon1
Exon2
Exon4
Exon1
Exon4
Exon2
Exon4
E
Con
clamp^delPrLD/clamp^delPrLD+6Q
Female
Male
Female
Male
R1 R2 R3 R1 R2 R3 R1 R2 R3 R1 R2 R3
unspliced
spliced
hrp38
gapdh
F
p=0.03
p=1.02 e-06
p=0.02
p=0.0937
Ratio between hrp38 isoforms (spliced vs unspliced)
30
25
20
15
10
5
0
Female
Male
Female
Male
Con
clamp^delPrLD/ clamp^delPrLD+6Q
G
CLAMP^WT
0 3.1 6.2 12.5
0 3.1 6.2 12.5 uM
Protein + RNA (Bound RNA)
Unbound RNA
Unbound RNA
hrp38 exon1 RNA (50nM)
hrp38 exon2 RNA (50nM)
H
CLAMP^WT
CLAMP^delPrLD
0 3.1 6.2 12.5
0 3.1 6.2 12.5 uM
Protein + RNA (Bound RNA)
Unbound RNA
Unbound RNA
hrp38 exon1 RNA (50nM)

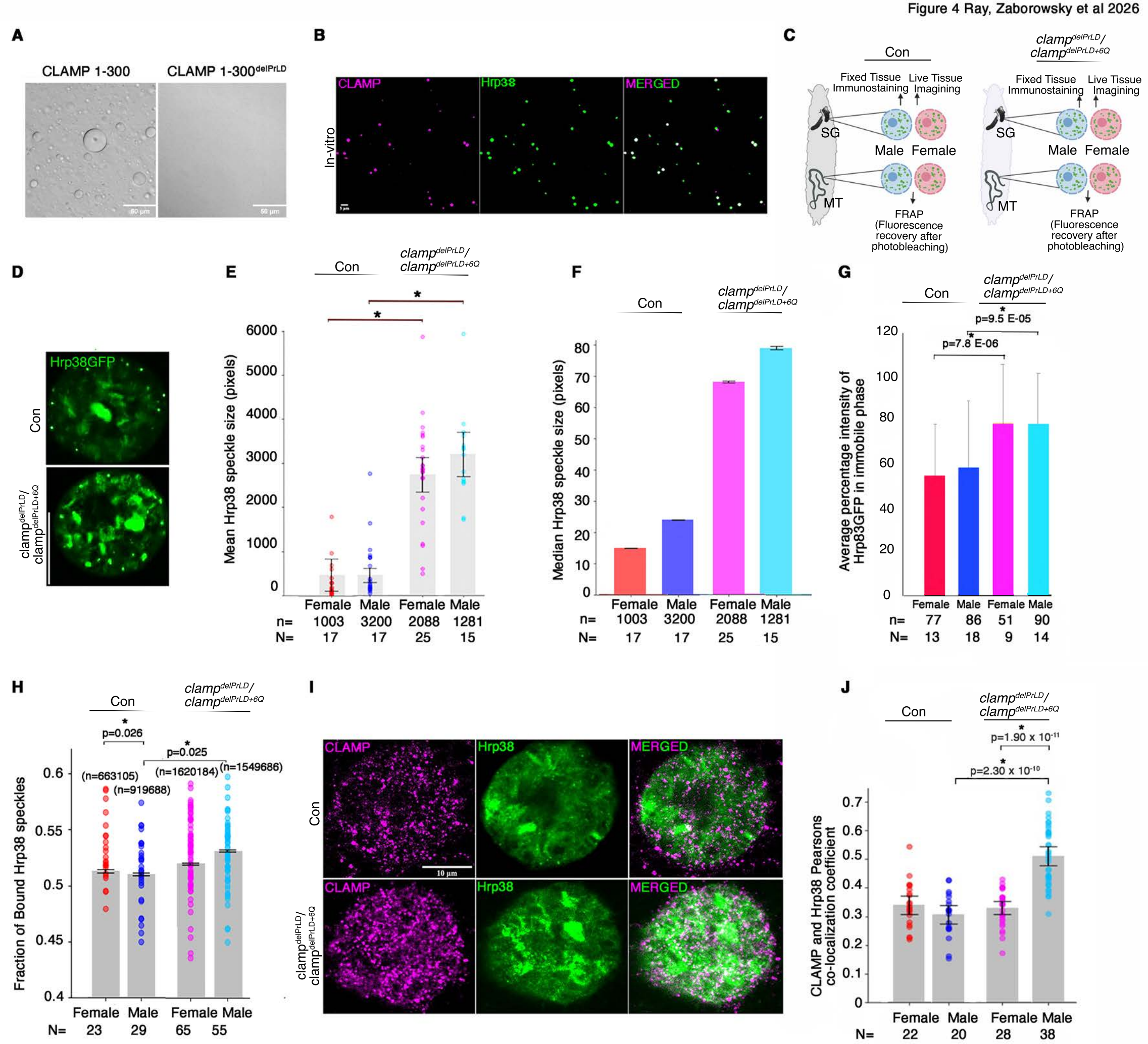
A
CLAMP 1-300
CLAMP 1-300delPrLD
B
CLAMP
Hrp38
MERGED
In-vitro
C
Con
clampdelPrLD/ clampdelPrLD+6Q
Fixed Tissue Immunostaining
Live Tissue Imagining
SG
Male Female
MT
FRAP (Fluorescence recovery after photobleaching)
D
Hrp38GFP
Con
clampdelPrLD/ clampdelPrLD+6Q
E
Mean Hrp38 speckle size (pixels)
Female Male Female Male
n= 1003 3200 2088 1281
N= 17 17 25 15
F
Median Hrp38 speckle size (pixels)
Female Male Female Male
n= 1003 3200 2088 1281
N= 17 17 25 15
G
Average percentage intensity of Hrp83GFP in immobile phase
p=9.5 E-05
p=7.8 E-06
Female Male Female Male
n= 77 86 51 90
N= 13 18 9 14
H
Fraction of Bound Hrp38 speckles
p=0.026
p=0.025
(n=663105)
(n=919688)
(n=1620184)
(n=1549686)
Female Male Female Male
N= 23 29 65 55
I
CLAMP
Hrp38
MERGED
10 µm
J
CLAMP and Hrp38 Pearsons co-localization coefficient
p=1.90 x 10-11
p=2.30 x 10-10
Female Male Female Male
N= 22 20 28 38